Oxidation state of iron and Fe-Mg partitioning between olivine and basaltic Martian melts

Revision 2

Andrew K. Matzen[1*]

Alan Woodland[2]

John R. Beckett[3]

Bernard J. Wood[1]

[1]University of Oxford, Department of Earth Sciences, Oxford, OX1 3AN, U.K.

[2] Goethe-Universität Institut für Geowissenschaften, Frankfurt, DE D-60438, Germany

[3]California Institute of Technology, MC 170-25, Pasadena, CA 91125, U.S.

*Corresponding author.

E-mail: andrew.matzen@earth.ox.ac.uk

For submission to

American Mineralogist

June 28, 2021

This is the peer-reviewed, final accepted version for American Mineralogist, published by the Mineralogical Society of America.
The published version is subject to change. Cite as Authors (Year) Title. American Mineralogist, in press.
DOI: https://doi.org/10.2138/am-2021-7682. http://www.minsocam.org/

ABSTRACT

We performed a series of experiments at 1 atmosphere pressure and temperatures of 1300-1500°C to determine the effect of oxygen fugacity on the oxidation state of Fe in a synthetic Martian basalt. Ferric-ferrous ratios were determined on the quenched glasses using Mössbauer spectroscopy. Following the conventional doublet assignments in the spectrum we obtain, at 1450°C, a $Fe^{3+}/\sum Fe$ of 0.19 at an oxygen fugacity corresponding to the QFM buffer. If, in contrast, we follow the Berry et al. (2018) assignments the calculated $Fe^{3+}/\sum Fe$ drops to 0.09, and the slope of the $log\left(X^{melt}_{FeO_{1.5}}/X^{melt}_{FeO}\right)$ *versus* $log(fO_2)$ changes from 0.18 to 0.26.

We used the oxidation state data, together with results of one additional olivine-bearing experiment to determine the appropriate value(s) for the olivine (ol)-liquid (liq) exchange coefficient, $K_{D,Fe^{2+}\text{-}Mg} = (FeO/MgO)^{ol}/(FeO/MgO)^{liq}$ (by weight). Our work suggests a $K_{D,Fe^{2+}\text{-}Mg}$ of 0.388 ± 0.006 (uncertainty is one median absolute deviation) using the traditional interpretation of Mössbauer spectroscopy and, a value of 0.345 ± 0.005 following the Mössbauer spectra approach of Berry et al. (2018). These results are broadly consistent with olivine-liquid partitioning data from the literature; using O'Neill et al. (2006) to estimate the Fe^{3+} content of experiments (an approach consistent with the traditional Mössbauer interpretation) gives a $K_{D,Fe^{2+}\text{-}Mg}$ of 0.365 ± 0.016; using O'Neill et al. (2018) to estimate the Fe^{3+} content of experiments (an approach consistent with the Berry et al. (2018) Mössbauer interpretation) yields a $K_{D,Fe^{2+}\text{-}Mg}$ of 0.359 ± 0.016.

We used our value of $K_{D,Fe^{2+}\text{-}Mg}$ to test whether any of the olivine-bearing shergottites represent liquids. For each meteorite, we assumed a liquid composition equal to that of the bulk, and then compared that liquid to the most Mg-rich olivine reported. Applying a $K_{D,Fe^{2+}\text{-}Mg}$ of

~0.36 leads to the possibility that bulk Yamato 980459, NWA 5789, NWA 2990, Tissint, and EETA 79001 (lithology A) represent liquids.

INTRODUCTION

The partitioning of elements between solid and liquid phases is an important tool for understanding and modeling igneous processes; relationships involving olivine are of particular interest due to its presence in a broad range of mafic and ultramafic lavas on the Earth and other planetary bodies (e.g., BVSP, 1981) and to its relatively simple major element chemistry. In a landmark study, Roeder and Emslie (1970) found that the olivine (ol)-liquid (liq) exchange coefficient, $K_{D,Fe^{+2}-Mg} = (FeO/MgO)^{ol}/(FeO/MgO)^{liq}$ is 0.30 ± 0.03 for basaltic compositions and independent of temperature between 1150 and 1300°C. The canonical value of 0.30 is still employed in both terrestrial and Martian applications (e.g., Falloon et al., 2007; Peslier et al., 2010, respectively), even though it has been challenged as being too low (e.g., Matzen et al., 2011). It is also important to note that liquid composition can have a significant effect on $K_{D,Fe^{+2}-Mg}$ (e.g., Ford et al., 1983; Gee and Sack, 1988; Toplis, 2005), which may limit the applicability of any specific value. Moreover, experimental work on terrestrial magmas (summarized by Matzen et al., 2011), Martian melt compositions (summarized by Filiberto and Dasgupta, 2011), eucrites (Stolper, 1977), and low-Ti lunar model compositions (Longhi et al., 1978; Seifert et al., 1988) indicate that a $K_{D,Fe^{+2}-Mg}$ of 0.33, or higher, is appropriate for many applications. Choice of the correct value of $K_{D,Fe^{+2}-Mg}$ is important for many specific applications. For example, Fe-Mg partitioning can be used as a criterion of equilibrium in experiments (e.g., Filiberto et al., 2010b) and for the estimation of parental liquid compositions

This is the peer-reviewed, final accepted version for American Mineralogist, published by the Mineralogical Society of America.
The published version is subject to change. Cite as Authors (Year) Title. American Mineralogist, in press.
DOI: https://doi.org/10.2138/am-2021-7682. http://www.minsocam.org/

which allows the calculation of mantle potential temperatures (e.g., Falloon et al., 2007; Putirka et al., 2007), as well as putative mantle compositions capable of producing observed magmas.

Although measurement of the olivine-liquid $K_{D,Fe^{+2}-Mg}$ relies (typically) on microprobe determination of olivine and glass compositions, the Fe content of the glass must be divided into $Fe^{2+}O$ and $Fe^{3+}O_{1.5}$ because the concentrations of both valences in the liquid are non-negligible at the conditions under which magmas on the Earth and Mars are believed to have formed and evolved (e.g., Cottrell and Kelley, 2011; Tuff et al., 2013). Measuring Fe^{3+}/Fe^{2+} in silicate liquids is difficult; as a result, Fe^{3+}/Fe^{2+} of a melt it is often assumed to be negligible (e.g., Filiberto and Dasgupta, 2011) or calculated using prior experimental calibrations (e.g., Sack et al. 1980, Jayasuriya et al. 2004). Given that these calibrations are largely based on terrestrial compositions, however, it is possible that their application to the high-Fe and low-Al Martian basalt compositions (Righter et al., 2013) introduces systematic errors into calculated Fe^{3+}/Fe^{2+}, and the resulting $K_{D,Fe^{+2}-Mg}$ values.

To more accurately constrain Fe^{3+}/Fe^{2+} in magmatic liquids, and the corresponding $K_{D,Fe^{+2}-Mg}$, of Martian basalts, we conducted a series of experiments at controlled temperature and oxygen fugacity (fO_2) on a synthetic analog of a proposed primary Martian basalt. After quenching, Fe^{3+}/Fe^{2+} ratios of the resultant glasses were determined by Mössbauer spectroscopy. We then combined our data with experiments from the literature to—after estimating the relative proportions of Fe^{3+} and Fe^{2+} in the liquid—determine an appropriate $K_{D,Fe^{+2}-Mg}$ value for Martian magmas. Finally, we used our value of $K_{D,Fe^{+2}-Mg}$ to determine which, if any, of the olivine-phyric shergottites potentially represent liquids.

This is the peer-reviewed, final accepted version for American Mineralogist, published by the Mineralogical Society of America.
The published version is subject to change. Cite as Authors (Year) Title. American Mineralogist, in press.
DOI: https://doi.org/10.2138/am-2021-7682. http://www.minsocam.org/

EXPERIMENTAL AND ANALYTICAL TECHNIQUES

Experimental Strategy/Overview

Most experiments were performed under superliquidus conditions to ensure equilibration of Fe^{3+}/Fe^{2+} in the melt with the flowing CO-CO_2 mixture was rapid (e.g., Thornber et al., 1980), and that experiments should (and did) quench to crystal-free glasses, facilitating the measurement of Fe^{3+}/Fe^{2+} by Mössbauer spectroscopy. In one group of experiments, the temperature was held approximately constant (~1450°C) and the *log* of the fO_2 varied between −10 (4.2 $\log_{10}$ units below the quartz-fayalite-magnetite buffer, defined by O'Neill (1987), QFM −4.2) and −0.68 (QFM +5.1) in order to determine if the available Fe^{3+}/Fe^{2+} models accurately describe our observations. In the second series of experiments, the fO_2 was held approximately constant, relative to the QFM buffer, and temperature varied from 1300 to 1500°C. Combining these two series of experiments allows us to infer the Fe^{3+}/Fe^{2+} ratio of our melt under arbitrary conditions and, to the extent our selected bulk composition is representative of Mars-appropriate melts, we can also determine an accurate $K_{D,Fe^{+2}-Mg}$ for olivine and glass (or a bulk composition being tested as a possible liquid) extracted from a Martian rock.

Starting compositions

Our initial composition was based on the average of the estimated Home Plate primitive magma compositions reported by Filiberto and Dasgupta (2011). To avoid time-dependent alkali loss in the one-atmosphere furnace (e.g., Corrigan and Gibb, 1979; Tsuchiyama et al., 1981), Na_2O was excluded and K_2O was replaced with an equal amount of NiO to facilitate a separate project on the partitioning of Ni between olivine and melt. This target composition was re-normalized and named MB1 (see Table 1). A mixture was prepared using high-purity oxides and carbonates that were combined and ground in an agate mortar under ethanol for approximately

2.5 hours, followed by decarbonation at 800°C in air overnight and, in some cases, reduction (see below). Our Fe^{3+}/Fe^{2+} equilibration experiments were performed using this bulk composition. Reconnaissance experiments on MB1 showed that low-calcium pyroxene, with an Mg# ~78 [Mg# = Mg/(Mg+Fe), atomic], is the liquidus phase, appearing between 1250 and 1300°C. To ensure olivine saturation at the liquidus, we added ~17% synthetic olivine (enough to ensure olivine saturation and that the experiment remained dominated by liquid, to help facilitate rapid equilibration) with an Mg# of 77 (the estimated Mg# of olivine in the primitive Martian mantle; Filiberto and Dasgupta 2011). This new bulk composition was named MB2. We refer to the as-synthesized and analyzed starting materials based on MB1 and MB2 as Syn-MB1 and Syn-MB2, respectively (see Table 1).

Experimental Techniques

After decarbonation, splits of the MB1 and MB2 starting materials were reduced at 900°C, either at an fO_2 corresponding to the QFM buffer or to 5 log_{10} units below the QFM buffer (QFM−5) for 2–5 hrs. Experiments run in air used unreduced starting material; experiments where QFM ≤ fO_2 < air used the powder reduced at QFM, and experiments more reducing than QFM used the powder reduced at ~QFM −5. Powdered starting materials were pressed into ~4 mm thick 13 mm diameter pellets using ethanol as a binder and pieces of pellet (generally between 50 and 140 mg) were loaded onto wire loops constructed using 0.25 mm diameter Pt or Re wire (see Table 2). Loop material for a particular experiment was chosen as a compromise between the lower Fe solubility in Re, compared to Pt at a given fO_2, and the increasing volatility of Re with increasing fO_2 (e.g., Borisov and Jones, 1999; Grove, 1981). We also mitigated Fe loss from the sample to the loop through pre-conditioning with two or more doping experiments, usually 12 hours in duration, using the same starting material held at the

same temperature and fO_2 on each loop prior to the experiments reported in Table 2. After a pre-conditioning experiment, the silicate bead was physically removed from the loop and the loop was cleaned by soaking in room-temperature hydrofluoric acid.

Experiments were introduced into the hot spot of a vertical one-atmosphere furnace at ~850ºC with the mixed gas selected for the experiment already flowing. fO_2 was controlled by flowing CO-CO_2 mixtures or air with a total flow rate of ~200 ml/min. Gas mixes were set, using mass-flow controllers, to give the desired fO_2 at the final run temperature. In most experiments (see Table 2 for exceptions), fO_2 was monitored using a yttria-stabilized zirconia oxygen sensor. Temperature was monitored using a type-B thermocouple, calibrated against the melting point of gold. Temperature was ramped from ~850°C to the final run temperature at a rate of 400–500º hr^{-1}; note that the time it took to reach the final run temperature is not included in the run times reported in Table 2. Experiments were drop quenched into a beaker of deionized water. Chips of recovered glass were mounted in epoxy for analysis with the electron microprobe, and splits of glass were ground, mixed with sugar, and pressed into pellets for analysis with Mössbauer spectroscopy.

Analytical Techniques

Glasses, and olivines were analyzed using a JEOL-8600 electron microprobe at the University of Oxford School of Archaeology and data were reduced using a PAP procedure (Pouchou and Pichoir, 1988). An accelerating voltage of 15 kV, beam currents of 10 and 40 nA, and spot sizes of 10 and 1 μm were used for glasses and olivines, respectively. Counting times ranged from 30 to 60 s on peak and half of that for backgrounds. MPI-DING glass GOR 128 (Jochum et al., 2006) was analyzed periodically during each glass analytical session as a secondary standard; in all probe sessions, the average composition for GOR 128 was within error

of the preferred value reported by Jochum et al. (2006). Olivine analyses were only accepted if their totals fell in the range 98.5-101.5 and yielded 3.000 ± 0.015 cations per formula unit.

Mössbauer spectra were recorded at room temperature (293 K) in transmission mode on a constant acceleration Mössbauer spectrometer with a nominal 1.85 GBq ^{57}Co source in a 6-micron Rh matrix. Glass samples were ground under acetone and packed either in a hole drilled in a Pb disc or in an acrylic holder. In order to minimize saturation effects, samples were prepared so that they had an Fe concentration of ~5 mg Fe cm^{-2}. A 25μm-thick Ta foil was mounted on the sample holder with a correspondingly large hole to improve the signal-to-noise ratio, since this metal absorbs ~99% of the 14.4 keV gamma-rays. The velocity scale was calibrated relative to 25 μm α-Fe foil. Mirror-image spectra were collected over 512 channels with a velocity range of ± 5 mm s^{-1}. The spectra were fitted using the commercially available NORMOS software package written by R.A. Brand (distributed by Wissenschaftliche Elektronik GmbH, Germany).

Mössbauer spectra of the glasses examined in this study consist of broad asymmetric doublets (Fig. 1), similar to the spectra of most silicate glasses (e.g., Cottrell et al., 2009; Virgo and Mysen, 1985). Two approaches were used in fitting the spectra to assess the sensitivity of $Fe^{3+}/\sum Fe$ to the fitting model. Method A employed extended Voigt-based line shapes with one-dimensional Gaussian distributions (σ_{CS}) for two Fe^{2+} doublets and one Fe^{3+} doublet. For each doublet, the center shift (CS), the Gaussian distribution width (σ_{CS}), and quadrupole splitting (QS) were allowed to vary. A two-dimensional fit including a Gaussian distribution in the quadrupole splitting was attempted, but proved to be unstable and did not converge. For all doublets, the Lorentzian linewidth was constrained to 0.19 mm s^{-1}. Method B simulated the approach of Berry et al. (2018), where fitting involved essentially a linear combination of a fixed

component for Fe^{2+} and another for Fe^{3+}. Here, we considered the spectra from run 30 to represent an endmember with only Fe^{2+} present since it was run at a $logfO_2$ of −10.0 (QFM −4.2). For this sample, we found that three doublets with extended Voigt-based line shapes with one-dimensional Gaussian distributions (σ_{CS}) were necessary to achieve a good fit (Berry et al. (2018) required only two Fe^{2+} doublets for their glass compositions). The Fe^{2+} component of spectra from samples run at higher fO_2 comprised these three doublets where the hyperfine parameters and the relative peak areas (1:0.39:0.088) were fixed, as defined by the fit to the spectrum from experiment 30. Then the Fe^{3+} component was accounted for by an additional doublet that also had an extended Voigt-based line shape with a one-dimensional Gaussian distribution (σ_{CS}). The Fe^{3+} doublets also had their Lorentzian linewidth fixed at 0.19 mm s^{-1}. Results for the two fitting methods are summarized in Table 2 and the hyperfine parameters are given in Table 3. Figure 1 shows the two methods applied to three representative spectra. In all cases, we estimate the error on $Fe^{3+}/\sum Fe$ to be 0.03. This error was assessed by comparing resulting ratios obtained using slightly different starting parameters and by comparing ratios obtained from samples with high Fe^{3+} contents that were fit using either one or two doublets for the ferric component (usually around ± 0.02). Our total uncertainty was increased slightly to account for any errors arising from non-zero sample thickness and other geometric effects.

RESULTS

The average measured compositions of the phases produced in our experiments are reported in Table 1, average glass compositions for individual experiments are reported in the electronic supplement. Mass-balance calculations (Table 2) suggest that our approach for avoiding Fe-loss to the sample holder (in this case a wire loop), which could result in local

perturbations to the ferric-ferrous ratios, was successful; most experiments (10 of 13) showing an absolute change in the total concentration of Fe of less than two percent relative. Run 30 exhibited the greatest change in iron concentration, with mass-balance calculations showing that it lost 5.7 percent of its Fe. In contrast, despite our pre-saturation experiments, significant amounts of Ni were lost from our silicate melt to both Pt and Re wires. For experiments conducted at ~1450ºC and similar run times, Ni losses increase with decreasing fO_2 for both container materials (Table 2); for our experiments, they are greater for Re than Pt but it should be kept in mind that Re loops were used under more reducing conditions. Given the correlation of Ni losses with fO_2 and the fact that impurity diffusion of Ni in Re is slower than is Ni in Pt (Boettinger et al., 2017; Eastman and Zhao, 2019) it seems likely that observed losses of Ni to sample containers are related to increasing Fe contents in the container alloys with decreasing fO_2.

Although the bulk compositions are nominally alkali-free, it is well-known that one-atmosphere experimental charges can acquire alkalis from contaminated furnace tubes (e.g., Matzen et al., 2011). Our experimental glasses were analyzed for alkalis and, when above the detection limit, are reported in Table 2. Alkali gains were modest; the maximum amount of Na_2O gained by a melt was 0.09 wt. % (Run 2-3).

In a first series of experiments, temperature was held approximately constant (~1450°C) and the *log* of the oxygen fugacity varied between −10.0 (QFM −4.2) and −0.68 (QFM +5.1); glasses show an increase in $Fe^{3+}/\sum Fe$ with increasing fO_2. For example, using "Method A" to fit Mössbauer spectra of the run product glasses (the same pattern is seen using Method B), the two experiments run at a *log* $fO_2 \sim -10$ (runs 30 and 57) have $Fe^{3+}/\sum Fe$ of 0.06–0.07 ± 0.03, whereas the experiment run in air (*log* fO_2 of −0.68) has a much higher $Fe^{3+}/\sum Fe$ ratio, 0.69 ± 0.03. For

experiments held near the QFM buffer (as defined by O'Neill, 1987), there is no significant change in $Fe^{3+}/\sum Fe$ with increasing temperature from 1300 to 1450°C, consistent with the results of O'Neill et al (2018). Runs 11, 13, 15, and 61 (1300 and 1450°C), for example, all have fO_2s that are within 0.1 *log* fO_2 units of the QFM buffer and Fe^{3+}/Fe^{total} of 0.19 (using Method A). Experiment 31 (1500°C), was run at a slightly higher *log* fO_2, QFM + 0.5, and has a slightly higher Fe^{3+}/Fe^{total} value of 0.22.

Our 1300°C experiment on Syn-MB2 contained 12% (by wt.) olivine and 88% glass. The olivine (Table 1) contains 41 wt. % MgO and 18 wt. % FeO, and the glass contains 13 wt. % MgO and 18 wt. % FeO* (FeO* = all Fe as FeO). It is crucial to note the similarity of the liquid produced in the experiment that used the Syn-MB2 starting material compared to those produced using the Syn-MB1 starting composition (see Table 1). Despite the addition of ~20 wt. % olivine to Syn-MB1 to construct Syn-MB2, the two liquids differ only by ~1.3 wt. % MgO, which suggests that our original starting composition was close to olivine saturation. Furthermore, we also note that the predicted difference in $\left(X_{FeO_{1.5}}^{melt} / X_{FeO}^{melt}\right)$ between Syn-MB1 and the glass of experiment 2-3, when calculated according to Jayasuriya et al. (2004; eqn. 12), is only 0.001. The similarity of these two liquids allows us to use Mössbauer measurements on olivine-free glasses to determine the valence of Fe in the olivine-bearing run product, and thus calculate an accurate $K_{D,Fe^{2+}-Mg}$. Using Method A to interpret the Mössbauer spectra leads to a $K_{D,Fe^{2+}-Mg}$ of 0.388 ± 0.006, whereas using Method B leads to a $K_{D,Fe^{2+}-Mg}$ of 0.345 ± 0.005.

DISCUSSION

Variation of ferric-ferrous ratio with oxygen fugacity

This is the peer-reviewed, final accepted version for American Mineralogist, published by the Mineralogical Society of America.
The published version is subject to change. Cite as Authors (Year) Title. American Mineralogist, in press.
DOI: https://doi.org/10.2138/am-2021-7682. http://www.minsocam.org/

An analysis of Fe-valence in magmatic liquids (e.g., Borisov et al., 2015; Fudali, 1965; Sack et al., 1980) generally begins with a statement such as

$$FeO^{melt} + 1/4\, O_2^{gas} \leftrightarrow FeO_{1.5}^{melt} \quad (1)$$

that connects the valence of iron with oxygen. At equilibrium, and at constant temperature and pressure, if the activity coefficients of FeO and $FeO_{1.5}$ are constant (or if their ratio is a constant), we would expect that a plot of $log\left(X_{FeO_{1.5}}^{melt} / X_{FeO}^{melt}\right)$ *versus* $log(fO_2)$ would yield a straight line with a slope of 0.25. Fudali (1965), however, found that the fO_2 dependence for magmatic liquids was significantly different from 0.25, with values exhibiting a "tendency to cluster" around 0.20. Sack et al. (1980) and Kress and Carmichael (1988) determined Fe^{3+}/Fe^{2+} using the same wet-chemical approach and found values of between 0.18 and 0.2, depending on the melt composition. More recently, Borisov et al., (2018) performed additional 1-atmosphere experiments, and made wet-chemical measurements of their own; their data, combined with previous wet-chemical measurements gives a slope of 0.207 ± 0.002. Subsequent studies, in which the ferric-ferrous ratios of experimentally-produced glasses were measured by Mössbauer spectroscopy, have also yielded slopes less than 0.25. For example, combining the Fe^{3+}/Fe^{2+} data for two basalts presented by Cottrell et al. (2009) and plotting against the *log* fO_2 gives a slope of 0.19 ± 0.01 (see Fig 2a). In an effort to determine the cause of the deviations in slope from the theoretical value of 0.25, Jayasuriya et al. (2004) performed a series of experiments on an anorthite-diopside eutectic composition to which they added only one wt. % FeO (an average terrestrial MORB has ~ 10 wt. %). They hypothesized that, if the deviation from a value of 0.25 were due to Fe^{2+} -Fe^{3+} interactions, then reducing the total iron content would result in an fO_2

term closer to 0.25. In this case, using Mössbauer spectroscopy to measure Fe oxidation state they, indeed, found a slope of 0.245 ± 0.004 (see Fig. 2b). The agreement with the theoretical relationship led them to fit existing ferric-ferrous data with an Fe^{2+} -Fe^{3+} interaction term and a slope fixed at the theoretical value. We should also note that Righter et al. (2013) performed a similar series of experiments on a synthetic Martian basalt, using Mössbauer spectroscopy to measure the ferric-ferrous ratios of their glasses. Their 1-atm experiments conducted at oxygen fugacities above QFM −2, at 1250ºC, yield a slope of 0.27 ± 0.07 (assuming that there is no difference in the recoil-free fraction of Fe^{2+} and Fe^{3+}). Note that in this study we assumed the recoil free fraction of ferric and ferrous iron were equal (e.g., Botcharnikov et al., 2005, and references therein). Recently, Zhang et al. (2018) have proposed a small recoil-free fraction correction for room-temperature spectra of basaltic glasses of 1.13 ± 0.07; applying this correction to our data does not change the slope of the ferric-ferrous ratio with oxygen fugacity (Fig. 2a, discussed below) and lowers the resulting $K_{D,Fe^{2+}-Mg}$ by only 0.008, a small amount compared to the uncertainty for this work (MAD for $K_{D,Fe^{2+}-Mg}$ in this work is 0.006). The principal reason we chose not to correct our data is that Zhang et al. (2018) show that are only very small differences, and no systematic differences, between Mossbauer spectra collected at 10K and at room-temperature for experimental glasses calibrated below QFM+2.5.

Recently, Berry et al., (2018) challenged the apparent agreement between the Mössbauer spectroscopy and wet-chemical measurements. Berry et al. (2018) performed experiments on an average MORB composition at a range of oxygen fugacities and measured the ferric-ferrous ratios of the resulting glasses with Mössbauer spectroscopy. The major difference between their results and those of previous authors is their interpretation of the Mössbauer spectra; they argue that the D2 doublet, which in iron-bearing silicate glasses was historically assigned to Fe^{3+}

(Method A e.g., Cottrell et al., 2009; Zhang et al., 2018), should be assigned to Fe^{2+} (Method B). The principal effects of such a reassignment are twofold; it decreases the Fe^{3+}/Fe^{2+} at moderate to low oxygen fugacities, and it changes the rate at which the ferric-ferrous ratio changes with oxygen fugacity. Berry et al. (2018) report that, for their data, assigning the D2 doublet to Fe^{2+} (model 3 from Berry et al. 2018), results in a slope of 0.26 ± 0.02, within error of the theoretical value of 0.25, whereas assigning the D2 doublet to Fe^{3+} results in a slope of 0.17-0.19. ± 0.02 (depending on the model used to fit the Mössbauer spectra). This presents a conundrum: reassignment of the D2 peak to Fe^{2+} results in a slope that is in good agreement with the theoretical value but it also makes their work inconsistent with a large body of previous experiments where the ferric-ferrous ratio was determined by wet-chemical analysis. At this stage, we are unable to discriminate between the two approaches so we have opted to apply both methods to our spectra and to calculate corresponding Fe-Mg olivine-liquid K_Ds. We should note, however, that several authors have expressed concerns about the Berry et al. (2018) fitting routine: Zhang et al. (2018) argued that the hyperfine parameters (quadrupole splitting and isomer shift) of the D2 feature are more consistent with Fe^{3+} in octahedral coordination (Dyar et al., 2006) than Fe^{2+}, as argued by Berry et al., (2018). Furthermore, Cottrell et al., (2020) point out that the linear-mixing routine employed by Berry et al., (2018) results in hyperfine parameters that do not change with ferric-ferrous ratio whereas previous work (e.g., Mysen, 2006, and references therein) often display a systematic variation of hyperfine parameters with ferric-ferrous ratio. In fact, there is no particular reason to assume that the local electronic environments around Fe^{2+} and Fe^{3+} atoms in a glass will be constant as concentrations change and modify their next-nearest neighbor configurations. All these considerations are consistent with our approach presented as Method A.

315

316 Figure 3 shows the measured ferric-ferrous ratios for our isothermal series. Using Method A to
317 fit our Mössbauer spectra results in a slope of 0.188 ± 0.019 (uncertainty reflects the 95%
318 confidence bounds), consistent with the fO_2 dependence found by previous authors (e.g., Cottrell
319 et al., 2009; Sack et al., 1980). Using Method B to fit our Mössbauer spectra (emulating the
320 approach of Berry et al., 2018), results in a slope of 0.260 ± 0.016, consistent with the 0.26 ±
321 0.02 reported by Berry et al. (2018). Note that the slopes for the new data presented here, as
322 with those reported from the literature, are derived from experiments run at fO_2s above QFM−2,
323 where Fe^{3+}/Fe^{2+} is unequivocally measurable (experiments excluded from the fits are shown on
324 Fig. 2 as open symbols). Also shown in Figure 3 are calculated results using some of the newest
325 and most widely-used models to predict ferric-ferrous ratios of melts. If Method A is used to
326 interpret our Mössbauer spectra, Jayasuriya et al. (2004), Borisov et al. (2018), and O'Neill et al.
327 (2006), who updated eqn. 14 from Jayasuriya et al. (2004), are consistent (i.e., within error) with
328 our ferric-ferrous data, with eqn. 12 of Jayasuriya et al (2004) performing the best. In the
329 absence of more extensive experimental data on Mars-relevant liquid compositions, we suggest
330 that these formulations are reasonable candidates for exploring the influence of bulk composition
331 on Fe^{3+}/Fe^{2+} in Martian igneous systems. Other proposed equations are less consistent with our
332 data. Kress and Carmichael's (1991) equation underestimates our observed ferric-ferrous ratios
333 at all oxygen fugacities by ~0.3 *log* units. The equation of Righter et al. (2013), although
334 formulated specifically for high-Fe melts like our synthetic Martian composition, consistently
335 underestimates the ferric-ferrous ratio by approximately one *log* unit. A possible source of this
336 disagreement is the magnitude of the Righter et al. (2013) temperature term: Most expressions of
337 $ln(Fe^{3+}/Fe^{2+})$ have temperature coefficients (10^4/T, K) close to or slightly above one (e.g.,

Jayasuriya et al., 2004; Kress and Carmichael, 1991; Sack et al., 1980 have temperature coefficients of 1.24, 1.15 and 1.31, respectively; see the supplement of Matzen et al. 2011), compared to 0.38 for the expression from Righter et al. (2013) at one atmosphere. Fe^{3+}/Fe^{2+} ratios based on Mössbauer Method B are close to those of O'Neill et al. (2018), who used similar spectral assignments and, as expected, are lower than those predicted by equations derived using traditional interpretation of Mössbauer data (Method A) and also those based on wet-chemical measurements (Fig 3).

Variation of ferric-ferrous ratio with temperature

Most of our experiments were conducted on Syn-MB1 at ~1450ºC. To investigate the effect of temperature on the ferric-ferrous ratio, we also did additional experiments at 1300 and 1500 ºC at oxygen fugacities near the QFM buffer [Fe^{3+}/Fe^{2+} of the 1500°C experiment at QFM+0.5 was corrected back to the value at QFM using the slope derived from the ~1450°C experiments (Fig 3)]. Both methods of interpreting the Mössbauer spectra lead to $Fe^{3+}/\sum Fe$ that are independent of temperature when oxygen fugacity is held constant (all values at QFM in the range of 0.184-0.194 for Method A and 0.081-0.097 for Method B). Most Fe^{3+}/Fe^{2+} equations from the literature correctly predict that, in the temperature range of our experiments, there is little change in the ferric-ferrous ratio at constant oxygen fugacity relative to the QFM buffer (O'Neill et al., 2018). Thus, one can use the ferric-ferrous ratios of natural glasses to infer the redox conditions at which they cooled, without a precise knowledge of the eruptive temperature, as long as the oxygen fugacity is expressed relative to the QFM buffer (e.g., Cottrell and Kelley, 2011; O'Neill et al., 2018).

Iron-Magnesium Exchange coefficients for Martian Basalts

Despite the widespread use of the "canonical" $K_{D,Fe^{2+}-Mg}$ of Roeder and Emslie (1970), who determined a value of 0.30, it has long been known that liquid composition can exert a significant effect on the iron-magnesium exchange coefficient (e.g., Ford et al., 1983; Gee and Sack, 1988). The main goal of our work is to measure both the ferric-ferrous ratio and the Fe-Mg partitioning between olivine and a silicate melt whose composition is modeled after a primitive Martian basalt. Combining the results of our super-liquidus experiments (which we used to measure ferric-ferrous ratios) with the results of our 1300°C experiment on Syn-MB2, which contained 12% (by wt.) olivine allows us to calculate a $K_{D,Fe^{2+}-Mg}$ of 0.388 ± 0.006 using Method A to interpret our Mössbauer spectra or 0.345 ± 0.005 using Method B.

We chose to omit Na and K from our starting composition because the loss of alkalis depends both on the duration (e.g., Corrigan and Gibb, 1979; Tsuchiyama et al., 1981) and the oxygen fugacity (e.g., Sossi et al., 2019) of the experiment, thereby making it easier for us to perform high-quality experiments. However, it is well known that alkalis can affect the Fe^{2+}-Mg exchange between olivine and liquid (e.g., Gee and Sack, 1988). Thus, a logical question is how applicable are the results of our work given that MB1 omits 3.12 wt. % Na_2O and and 0.43 wt.% K_2O that are observed in the target primitive Martian melt (Table 1). Looking, primarily, at terrestrially-inspired bulk compositions, Matzen et al. (2011) found that there appeared to be little change in the $K_{D,Fe^{2+}-Mg}$ for total alkalis (Na_2O + K_2O) below 5 wt. % (see their Fig. 6). Using their data, we estimate (by fitting a line to those experiments that have ≤ 5 wt. % Na_2O + K_2O) that by omitting Na_2O and K_2O from our starting composition we have increased the $K_{D,Fe^{2+}-Mg}$ by ~0.008. Given the small size of this effect (relative to analytical uncertainties; MAD for $K_{D,Fe^{2+}-Mg}$ in this work is 0.006), and the observation that olivine-phyric shergottites (discussed below) tend to have much lower total alkalis (LAR 06319 has the highest with 1.3 wt.

383 % $Na_2O + K_2O$), we are confident that the results of our work can be applied to Martian systems
384 with low (<4 wt. %) total alkalis.

385 Since our ferric/ferrous determinations using Method A and B should be consistent with
386 the model of O'Neill et al. (2006) and O'Neill et al. (2018), respectively, we can use these
387 expressions to estimate ferric-ferrous ratios in previously published olivine-saturated
388 experiments on Martian-inspired bulk compositions. The median $K_{D,Fe^{+2}-Mg}$ of 17 one-
389 atmosphere experiments on Martian bulk compositions (Filiberto et al., 2008; Herd et al., 2009)
390 whose analytical totals (post Fe^{+3}/Fe^{+2} correction for glasses) are between 98 and 102 wt. % is
391 0.354 ± 0.008 and 0.336 ± 0.009 (error is one mean absolute deviation, MAD), using O'Neill et
392 al. (2006) and (2018), respectively (Figure 5). Note that the median $K_{D,Fe^{+2}-Mg}$ of one-
393 atmosphere experiments calculated using O'Neill et al. (2006), 0.354 ± 0.008, is significantly
394 lower than the equivalent value (0.388 ± 0.006, Mössbauer-Method A) reported for this work.

395 Many experiments on Martian bulk compositions were conducted at high pressures (0.4-5
396 GPa) in an attempt to mimic the conditions of melting and crystallization in the Martian mantle
397 (e.g., Filiberto et al., 2010b; Gross et al., 2011; Usui et al., 2008). Following Médard et al.
398 (2008), Filiberto and Dasgupta (2011) noted that redox conditions in piston cylinder experiments
399 conducted using graphite capsules, which includes all of the high-pressure experiments being
400 considered here, are approximately 0.8 *log* fO_2 units more reducing than the graphite C-O buffer.
401 We excluded experiments performed at or below 1150°C because the results of experiments
402 from Nekvasil et al. (2009), McCubbin et al. (2008), and Filiberto (2008) all suggest a sharp
403 increase in $K_{D,Fe^{+2}-Mg}$ with decreasing temperature, from roughly 0.35 to 0.40 between ~1150
404 and 1000°C. A dramatic increase in $K_{D,Fe^{+2}-Mg}$ would be surprising given numerous studies

concluding that $K_{D,Fe^{+2}-Mg}$ is insensitive to changes in temperature (e.g., Matzen et al., 2011; Roeder and Emslie, 1970). It is important to note that low-temperature experiments are inherently difficult due to slow kinetics and the presence of multiple (≥4) phases. Further experimentation will be needed to assess whether the apparent increase in $K_{D,Fe^{+2}-Mg}$ at low temperatures is a property inherent to these experiments, or simply an experimental artifact reflecting a lack of equilibrium. We avoid these issues by considering only experiments run at or above 1150°C and restricting applications to temperatures at or above 1150°C. If we consider only the 66 high-pressure experiments run on Martian compositions at temperatures at or above 1150°C (Agee and Draper, 2004; Bertka and Holloway, 1994a; Blinova and Herd, 2009; Dann et al., 2001; Filiberto, 2008; Filiberto et al., 2010a; Filiberto et al., 2009; Filiberto et al., 2010b; Filiberto and Treiman, 2009; Filiberto et al., 2008; McCubbin et al., 2008; Monders et al., 2007; Musselwhite et al., 2006; Nekvasil et al., 2009) with oxide sums, after correcting for Fe^{+3}/Fe^{+2}, between 98-102 wt. %, the resulting median $K_{D,Fe^{+2}-Mg}$ is 0.365 ± 0.016 and 0.359 ± 0.016 (where uncertainty is one MAD) using the O'Neill et al. (2006) and (2018) expressions, respectively. These values are in good agreement with the $K_{D,Fe^{+2}-Mg}$s obtained from one-atmosphere experiments on Martian bulk compositions (0.354 ± 0.008 and 0.336 ± 0.009, respectively), and the results of our work (0.388 ± 0.006 and 0.345 ± 0.005, respectively, see Fig 5). Almost all results for $K_{D,Fe^{+2}-Mg}$, using either Fe^{+3}/Fe^{+2} model, are significantly greater than the canonical value of 0.30.

Olivine-phyric shergottites

Olivine-phyric shergottites are a subclass of shergottites thought to have originated in the interior of Mars and representing primary liquids or liquids modified through fractionation or

accumulation of olivine and other phases. Identification of primary liquids is important because it provides a means of estimating the compositions of the source regions of Martian magmas. A basic test for primary liquids is to suppose that the most forsteritic olivine observed in a shergottite corresponds to the first crystallizing olivine and that this olivine was in equilibrium with a liquid whose bulk composition matches that of the meteorite. If this supposition is correct, the apparent $K_{D,Fe^{+2}-Mg}$ computed from the bulk meteorite and olivine compositions should match the experimental value. We note that this supplies a necessary (olivine of observed composition is on the liquidus) but insufficient (the liquid must have suffered no fractionation/accumulation) test for a primary liquid.

In Figure 6, we compare Mg#s (where Mg#=Mg/[Fe^{+2}+Mg], atomic) of bulk olivine-phyric shergottites to the most Mg-rich olivine phenocrysts. To calculate the Mg# of the bulk, we determined Fe^{+3}/Fe^{+2}, using the models of O'Neill et al. (2006), panel a, and O'Neill et al. (2018), panel b, and reported bulk compositions (Anand et al., 2008; Barrat et al., 2002; Bunch et al., 2009; Dreibus et al., 2000; Filiberto et al., 2012; Filiberto et al., 2018; Funk, 2016; Herd et al., 2013; Irving et al., 2010; Irving et al., 2013; Kuehner et al., 2011; Mellin et al., 2008; Sarbadhikari et al., 2009; Shirai and Ebihara, 2004; Shirai et al., 2009; Taylor et al., 2002; Zipfel et al., 2000). We used maximum temperatures and oxygen fugacity estimates from the literature (Funk, 2016; Gross et al., 2013; Gross et al., 2011; Herd, 2003; McCanta et al., 2009; Peslier et al., 2010; Shearer et al., 2006), where available. If temperature and fO_2 estimates were both unavailable, we calculated the temperature using Beattie (1993) and assumed that the fO_2 ranged from 1 to 3.5 log_{10} units below the QFM buffer (Herd, 2003). Olivine compositions were taken from the literature (aforementioned bulk meteorite references and; Goodrich, 2002; Goodrich and Zipfel, 2001; Gross et al., 2013; Gross et al., 2010; Hsu et al., 2012; Irving et al., 2007;

Lapen et al., 2017; Mikouchi et al., 2008; Mikouchi et al., 2001; Papike et al., 2009; Peslier et al., 2010; Taylor et al., 2002; Usui et al., 2008); the results are shown in Fig. 6. Of the 18 olivine-phyric shergottites tested, five (Yamato 980459, NWA 2990, NWA 5789, Tissint, and EET 79001A) yield apparent $K_{D,Fe^{+2}-Mg}$ values consistent with the experimentally-determined values, leading to the possibility that these are primary liquid compositions. Meteorite NWA 7635 merits further research; as mentioned above, low-temperature (<1150°C) experiments on Martian bulk compositions show an increasing $K_{D,Fe^{+2}-Mg}$. NWA 7635 is evolved, as the bulk only has 4.11 wt. % MgO, giving estimates of the onset of olivine crystallization that are close to this temperature (1193°C using Beattie 1993 and 1127°C using the MgO-based thermometer of Matzen et al. 2011). Thus, further experiments are needed to determine if the apparent $K_{D,Fe^{+2}-Mg}$ of ~0.43 for this meteorite represents an equilibrium value. The other 12 shergottites lie so far off the predicted curve indicating that the bulk meteorites are not plausible liquids. These conclusions are similar to the those of Gross et al. (2011) and Filiberto and Dasgupta (2011).

Our work has identified five meteorites whose bulk compositions, according to Fe-Mg partitioning between olivine and liquid, represent possible liquid compositions. The next logical step is to see if these five meteorites share common attributes, or are different from the meteorites whose bulk compositions, according to our calculations, are not potential liquids. Unfortunately, there does not seem to be a reliable characteristic that separates those meteorites that fall near the equilibrium Fe-Mg partitioning line from those that do not. In fact, the five meteorites that fall near the equilibrium line have different rare-Earth element (REE) patterns (NWA 2990 is light-REE enriched while the rest are depleted), olivine sizes (up to 3 mm for NWA 5789 and 0.3 mm for NWA 2990), and apparent amounts of zoning in the olivines (with the caveat that zoning is often described more qualitatively). We also examined the major-

element concentration in the bulk of the five meteorites that we identify as potential liquids and compared them to those that fall away from the equilibrium line in Figure 6. Again, we find that the five potential liquids are indistinct from those that are not. For example, the median CaO/Al_2O_3 ratio of the potential liquids (1.26, with a minimum of 1.23 and a maximum of 1.34) is similar to those that are not (1.28 with a minimum of 0.86 and a maximum of 3.35).

An interesting feature of Figure 6 is that all of the meteorites that are not likely to be primary liquids lie above and to the left of the equilibrium $K_{D,Fe^{+2}-Mg} \approx 0.36$ line. There are a few possible explanations for this phenomenon: (1) the bulk may have accumulated olivine, or other Mg-rich phases (e.g., Filiberto and Dasgupta, 2011), (2) the olivine phenocrysts may have diffusively re-equilibrated with their more Fe-rich rims, or (3) we have, simply, not found the most Mg-rich phenocryst. We believe that finding the most-Mg rich olivine phenocryst may be problematic due to the fact that olivine phenocrysts are often zoned (e.g., Peslier et al., 2010) but accumulation of Mg-rich phases is a commonly-observed phenomenon and is likely to be largely responsible for the disequilibrium $K_{D,Fe^{+2}-Mg}$ values.

IMPLICATIONS

We find that the oxygen-fugacity dependence of Fe^{3+}/Fe^{2+} in a model Martian basalt is consistent, on a *log-log* plot with the theoretical slope of 0.25, if we follow the Berry et al. (2018) approach to fitting the Mössbauer spectra and assign the D2 doublet to Fe^{2+} rather than Fe^{3+} (Method B). If, however, we follow convention and assign this to Fe^{3+} (Method A) then Fe^{3+}/Fe^{2+} values are significantly higher and the slope is 0.188 ± 0.019 consistent with both earlier results using the same approach to interpreting the Mössbauer spectra and with wet-chemical measurements of ferric-ferrous ratios in quenched melts.

For oxygen fugacities at the QFM buffer, there is no detectable change of oxidation state for our experiments in the temperature range 1300-1500^{o}C at 1 atmosphere pressure. $Fe^{3+}/\sum Fe$ ratios of the Martian basalt at QFM average 0.19 if we apply Method A and 0.09 if we use Method B.

We determined the olivine-melt $K_{D,Fe^{+2}-Mg}$ for the synthetic Martian basalt with values of 0.388 (ferric/ferrous Method A) and 0.345 (Method B). Combining our results with data from the literature we tested whether any of the olivine-phyric shergottites are conceivably primary liquids. We find that five such meteorites (Yamato 980459, NWA 2990, NWA 5789, Tissint, and EETA 79001A) have apparent $K_{D,Fe^{+2}-Mg}$ values of approximately 0.36 and are hence potential primary liquid compositions.

ACKNOWLEDGEMENTS

We would like to thank Victoria Smith for her efforts to run and maintain the electron microprobe laboratory, Steven Wyatt for hood space and safe HF handling, and Jamie Long, and all the other workshop technicians, who help to keep the experimental laboratory running. We would also like to thank Maryjo Brounce, Elizabeth Cottrell, and Glenn Gaetani for thoughtful and through reviews.

FUNDING

This research began with support from ERC Advanced Grant 267764 and was completed with support from STFC (UK) grant ST/R000999/1

FIGURE CAPTIONS

FIGURE 1. Mössbauer spectra of three representative samples; data are shown as black circles. For each sample, fits to the spectra (magenta) using Method A are shown on the left (panels a, c, and e), and Method B on the right (panels b, d, and f). Ferrous doublets are shown in aqua and ferric doublets are orange. Residuals (data less the fit) are shown as a light blue line offset to 1.005.

FIGURE 2. *Log* of ferric-ferrous ratio *vs*. *log* fO_2 relative to the QFM buffer. Panel a shows 1460 and 1360°C data for basalt JDFD2 (black circles) from Kress and Carmichael (1988) along with the two basalts from Cottrell et al. (2009) as blue triangles; ordinary least squares fits, and the resulting slopes are shown in black and blue, respectively. Panel b shows data from Berry et al. (2018) and Jayasuriya et al. (2004) as black diamonds and red squares, respectively; ordinary least squares fits to solid symbols, and the resulting slopes are shown in black and red, respectively. Experiments conducted below QFM −2 were excluded from the fit (shown on the plot as open/unfilled symbols) due to the increasing errors in ferric-ferrous ratio at low fO_2. Errors represent 95% confidence bounds on the coefficients obtained from the fit. A reference slope of 0.25 is shown on each panel as a black dashed line.

FIGURE 3. Iron redox state from this work (Method A and B) compared to a selection of recent and widely used predictions from the literature (Borisov et al., 2018; Jayasuriya et al., 2004; Kress and Carmichael, 1991; O'Neill et al., 2018; O'Neill et al., 2006; Righter et al., 2013) computed using the composition of our experimental glass. Note that in both panels the Method B measurements are offset by 0.05 *log* units for clarity.

FIGURE 4. *Log* (Fe^{3+}/Fe^{2+}) in the melt as a function of temperature. Data points from this study were corrected for small deviations from the QFM buffer using the Fe^{3+}/Fe^{2+} *vs*. fO_2 slopes for each Method. Literature sources as in Fig. 3.

FIGURE 5. $D_{Fe^{+2}}=FeO^{ol}/FeO^{liq}$ *versus* $D_{Mg}=MgO^{ol}/MgO^{liq}$ (both by wt.) for one-atm (filled black circles: this study; open squares: literature) and high-pressure (blue circles) along with lines of constant $K_{D,\,Fe+2\text{-}Mg}$. High-pressure experiments were taken from the following sources: (Agee and Draper, 2004; Bertka and Holloway, 1994a; Bertka and Holloway, 1994b; Blinova and Herd, 2009; Dann et al., 2001; Filiberto, 2008; Filiberto et al., 2010a; Filiberto et al., 2009; Filiberto et al., 2010b; Filiberto et al., 2008; McCubbin et al., 2008; Monders et al., 2007; Musselwhite et al., 2006; Nekvasil et al., 2009). One-atm experiments were taken from Filiberto et al. (2008) and Herd et al. (2009). Fe^{3+} contents of silicate liquids were estimated using O'Neill et al. (2006) in panel a, and O'Neill et al. (2018) in panel b.

FIGURE 6. Mg# of a liquid equal in composition to that of the bulk of the meteorite as a function of the Mg# of the most Mg-rich observed olivine. Constant $K_{D,Fe^{+2}-Mg}$ contours are also shown. For each meteorite, we calculate the Mg# of the bulk using the Fe^{3+} contents of the assumed liquid using O'Neill et al. (2006) in panel a, and O'Neill et al. (2018) in panel b. Where available, we use estimated maximum temperatures and fO_2s. For meteorites where estimated fO_2s are not available, we show a bar corresponding to QFM−1 to QFM−3. Our results suggest that bulk compositions of NWA 5789, NWA 2990, EETA 79001A, Tissint, and Y980459 represent possible liquids.

This is the peer-reviewed, final accepted version for American Mineralogist, published by the Mineralogical Society of America.
The published version is subject to change. Cite as Authors (Year) Title. American Mineralogist, in press.
DOI: https://doi.org/10.2138/am-2021-7682. http://www.minsocam.org/

562 **FIGURE 1.**

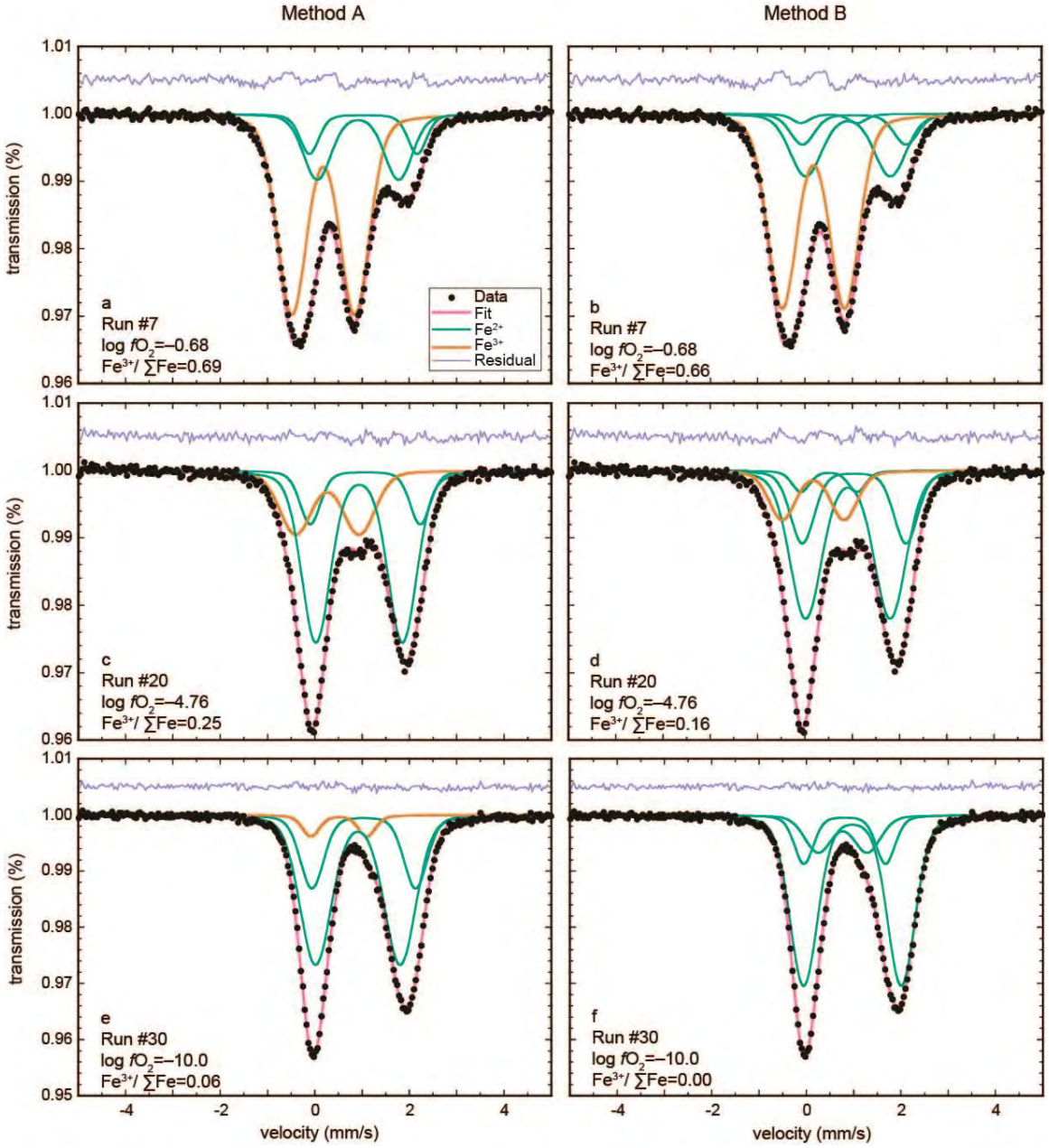

563
564
565
566
567
568
569
570
571
572

This is the peer-reviewed, final accepted version for American Mineralogist, published by the Mineralogical Society of America.
The published version is subject to change. Cite as Authors (Year) Title. American Mineralogist, in press.
DOI: https://doi.org/10.2138/am-2021-7682. http://www.minsocam.org/

573 **FIGURE 2.**
574

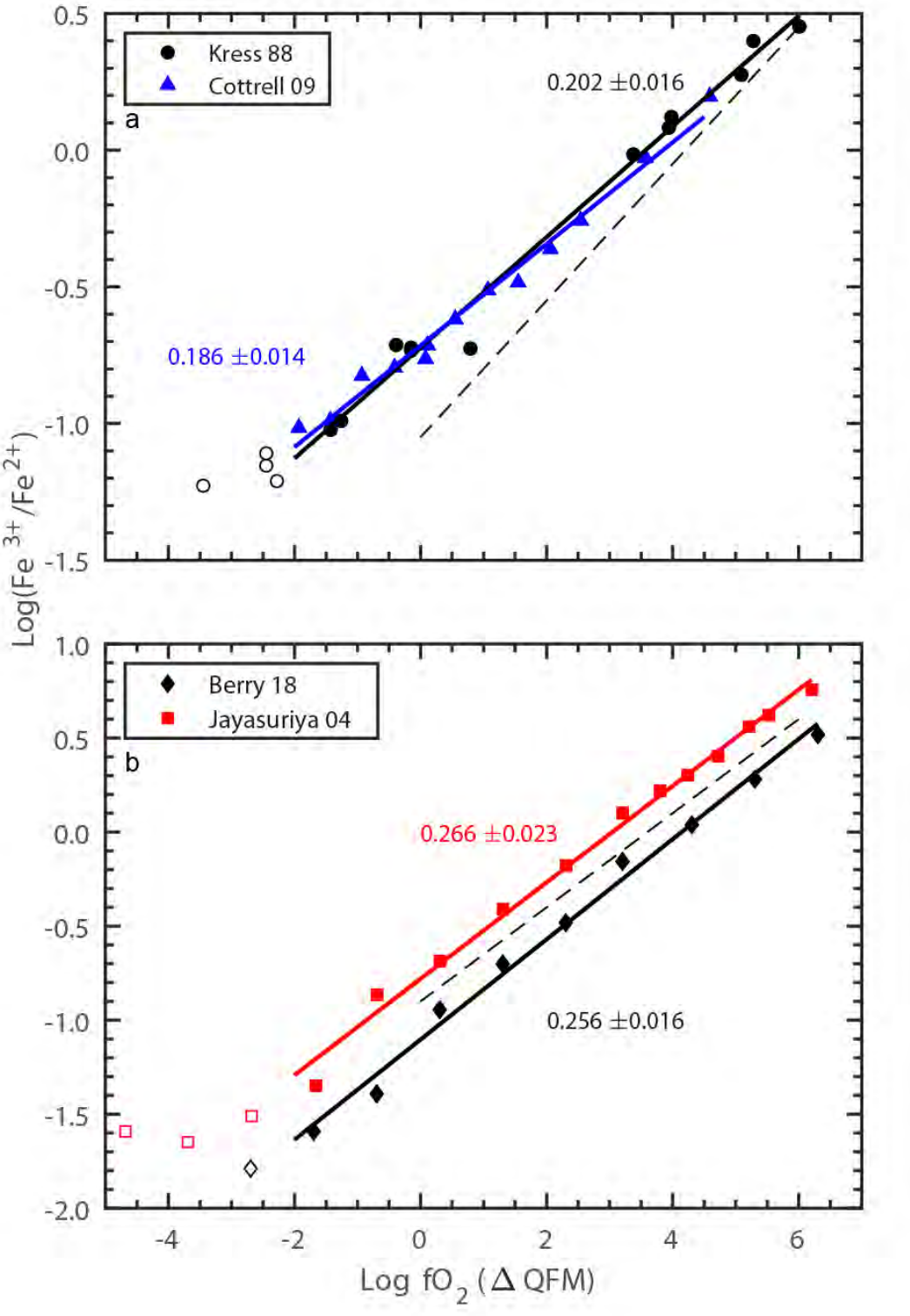

575
576
577

578 **FIGURE 3.**
579

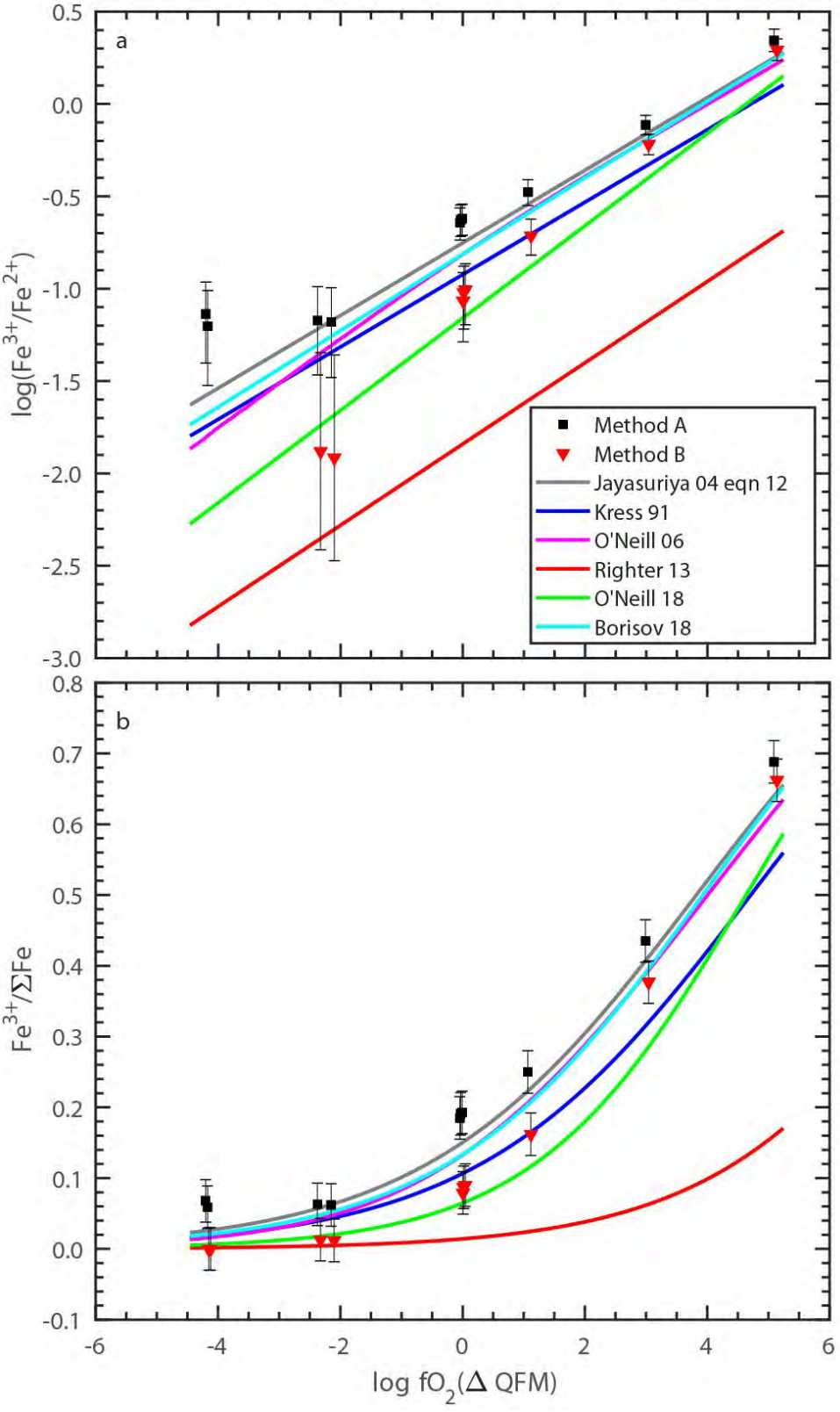

580
581

582 **FIGURE 4.**
583

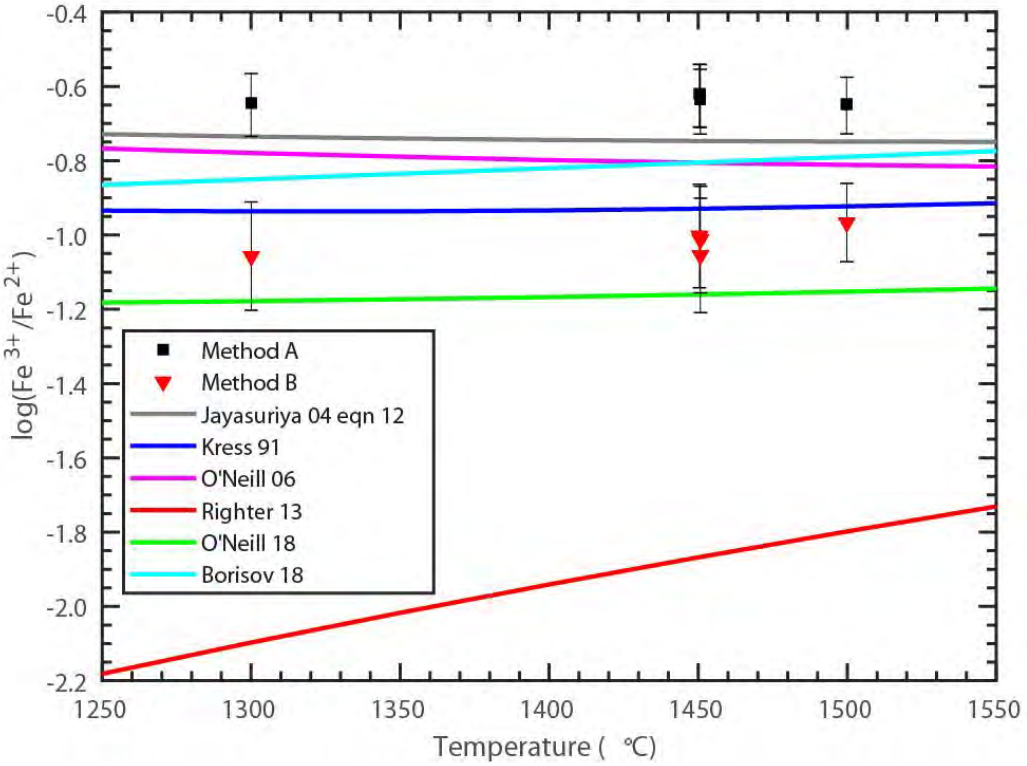

584
585
586
587
588
589
590
591
592
593
594
595
596

This is the peer-reviewed, final accepted version for American Mineralogist, published by the Mineralogical Society of America.
The published version is subject to change. Cite as Authors (Year) Title. American Mineralogist, in press.
DOI: https://doi.org/10.2138/am-2021-7682. http://www.minsocam.org/

597 **FIGURE 5.**

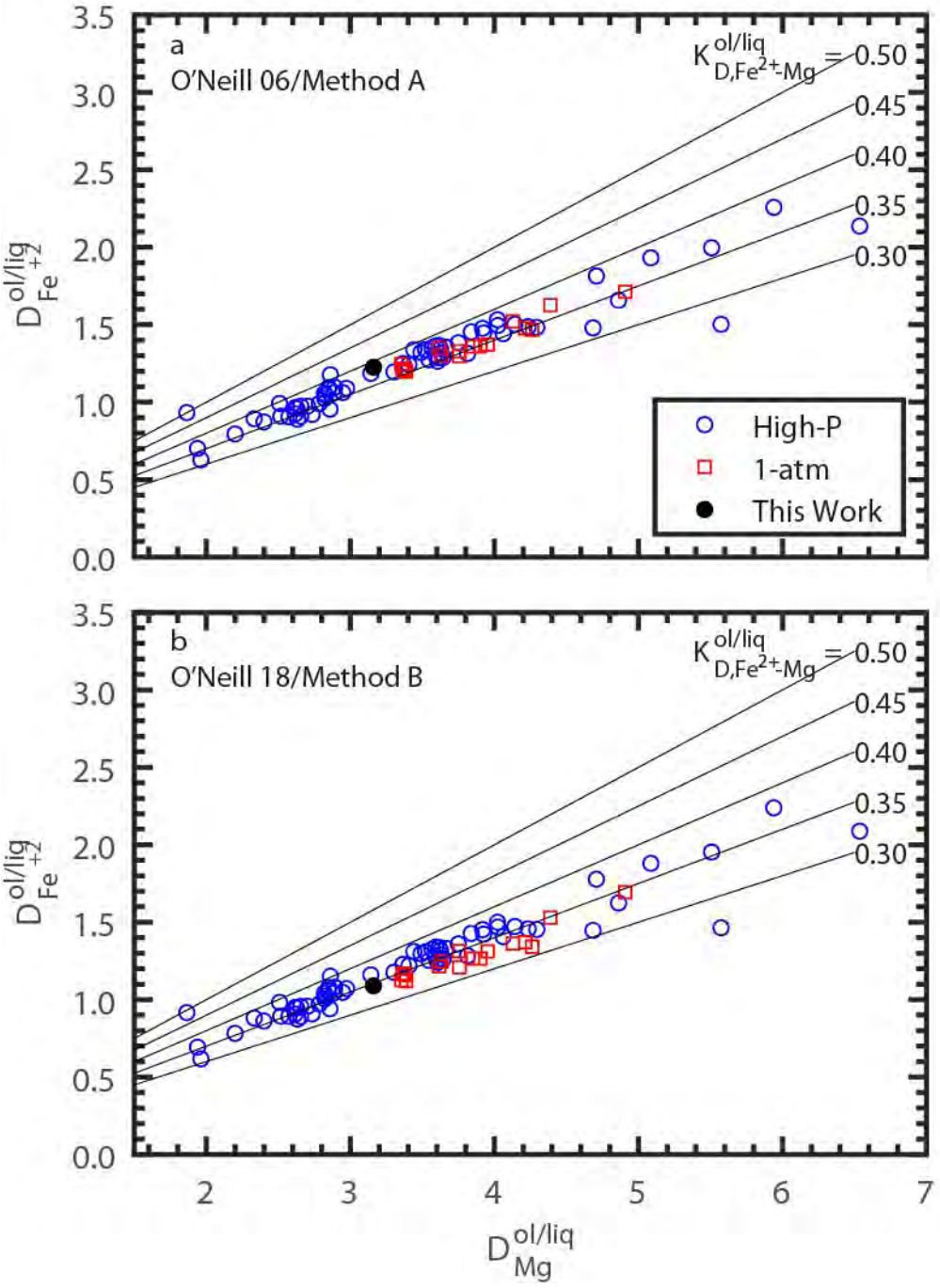

598
599
600
601

This is the peer-reviewed, final accepted version for American Mineralogist, published by the Mineralogical Society of America.
The published version is subject to change. Cite as Authors (Year) Title. American Mineralogist, in press.
DOI: https://doi.org/10.2138/am-2021-7682. http://www.minsocam.org/

602
603
604
605 **FIGURE 6.**

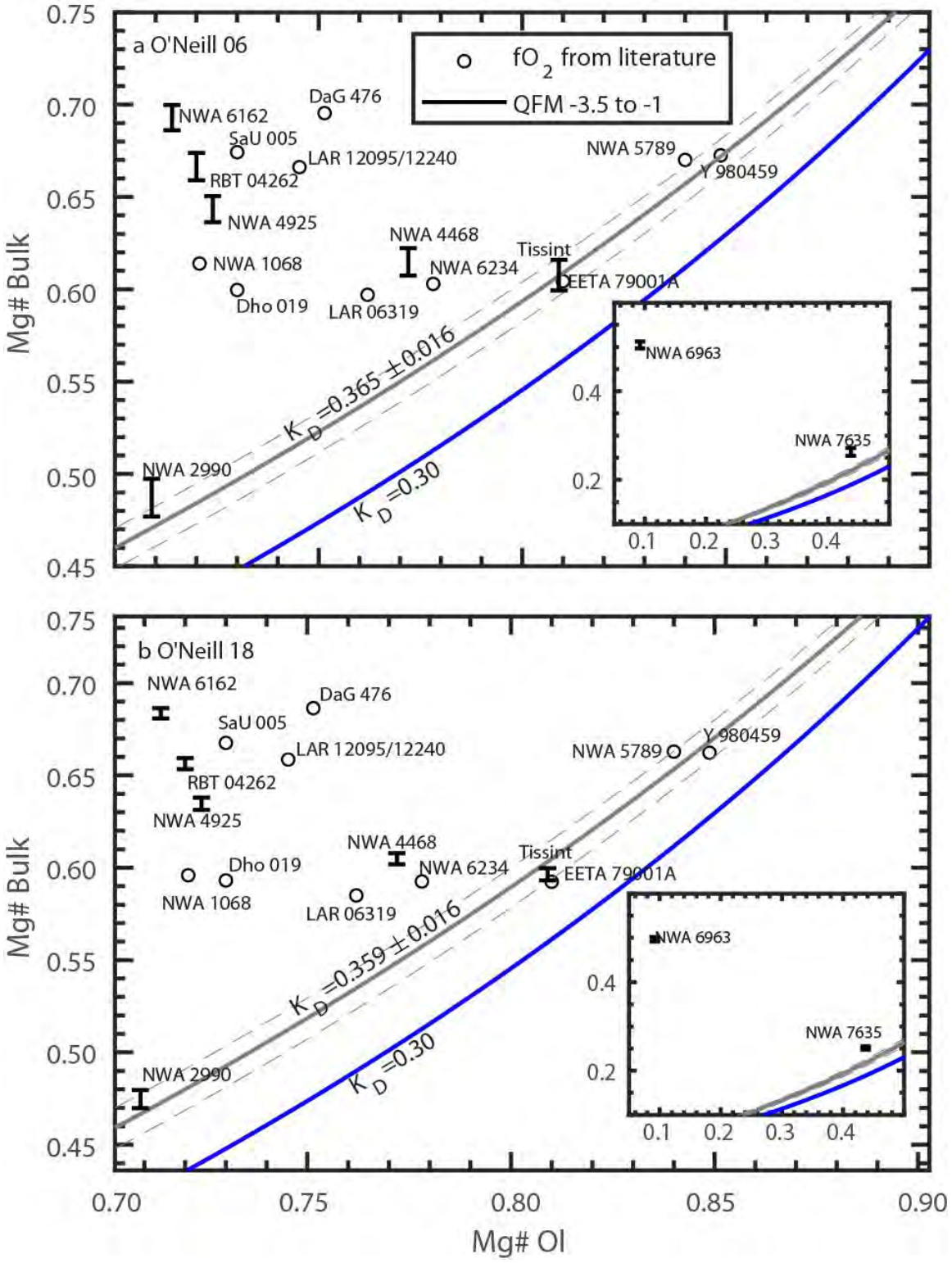

606
607

608
609
610
611

REFERENCES CITED

612 Agee, C.B., and Draper, D.S. (2004) Experimental constraints on the origin of Martian
613 meteorites and the composition of the Martian mantle. Earth and Planetary Science
614 Letters, 224, 415-429.
615 Albarède, F., and Provost, A. (1977) Petrological and geochemical mass-balance equations: an
616 algorithm for least-square fitting and general error analysis. Computers and Geosciences,
617 3, 309-326.
618 Anand, M., James, S., Greenwood, R.C., Johnson, D., Franchi, I.A., and Grady, M.M. (2008)
619 Mineralogy and geochemistry of shergottite RBT 04262. 39th Lunar and Planetary
620 Science Conference, abstract 2173.
621 Barrat, J.A., Jambon, A., Bohn, M., Gillet, P., Sautter, V., Göpel, C., Lesourd, M., and Keller, F.
622 (2002) Petrology and chemistry of the picritic shergottite North West Africa 1068 (NWA
623 1068). Geochimica et Cosmochimica Acta, 66, 3505-3518.
624 Beattie, P. (1993) Olivine-melt and orthopyroxene-melt equilibria. Contributions to Mineralogy
625 and Petrology, 115, 103-111.
626 Berry, A.J., Stewart, G.A., O'Neill, H.S.C., Mallmann, G., and Mosselmans, J.F.W. (2018) A re-
627 assessment of the oxidation state of iron in MORB glasses. Earth and Planetary Science
628 Letters, 483, 114-123.
629 Bertka, C.M., and Holloway, J.R. (1994a) Anhydrous partial melting of an iron-rich mantle I:
630 subsolidus phase assemblages and partial melting relations at 10 to 30 kbar.
631 Contributions to Mineralogy and Petrology, 115, 313-322.
632 Bertka, C.M., and Holloway, J.R. (1994b) Anhydrous partial melting of an iron-rich mantle II:
633 primary melt compositions at 15 kbar. Contributions to Mineralogy and Petrology, 115,
634 323-338.
635 Blinova, A., and Herd, C.D.K. (2009) Experimental study of polybaric REE partitioning between
636 olivine, pyroxene and melt of the Yamato 980459 composition: Insights into the
637 petrogenesis of depleted shergottites. Geochimica et Cosmochimica Acta, 73, 3471-3492.
638 Boettinger, W.J., Williams, M.E., Moon, K.W., McFadden, G.B., Patrone, P.N., and Perepezko,
639 J.H. (2017) Interdiffusion in the Ni-Re system: Evaluation of uncertainties. Journal of
640 Phase Equilibria and Diffusion, 38, 750-763.
641 Borisov, A., and Jones, J.H. (1999) An evaluation of Re, as an alternative to Pt, for the 1 bar loop
642 technique: An experimental study at 1400 °C. American Mineralogist, 84, 1528-1534.
643 Borisov, A., Behrens, H., and Holtz, F. (2015) Effects of melt composition on Fe^{3+}/Fe^{2+} in
644 silicate melts: a step to model ferric/ferrous ratio in multicomponent systems.
645 Contributions to Mineralogy and Petrology, 169, 24.
646 Borisov, A., Behrens, H., and Holtz, F. (2018) Ferric/ferrous ratio in silicate melts: a new model
647 for 1 atm data with special emphasis on the effects of melt composition. Contributions to
648 Mineralogy and Petrology, 173, 98.
649 Botcharnikov, R.E., Koepke, J., Holtz, F., McCammon, C., and Wilke, M. (2005) The effect of
650 water activity on the oxidation and structural state of Fe in a ferro-basaltic melt.
651 Geochimica et Cosmochimica Acta, 69, 5071-5085.

Bunch, T.E., Irving, A.J., Wittke, J.H., Rumble, D., III, Korotev, R.L., Gellissen, M., and Palme, H. (2009) Petrology and composition of Northwest Africa 2990; a new type of fine-grained, enriched, olivine-phyric shergottite. 40th Lunar and Planetary Science Conference, abstract 2274.

BVSP. (1981) Basaltic Volcanism on the Terrestrial Planets. 1286 p. Pergamon Press, Inc, New York.

Corrigan, G., and Gibb, F.G.F. (1979) Loss of Fe and Na from a basaltic melt during experiments using the wire-loop method. Mineralogical Magazine, 43, 121-126.

Cottrell, E., and Kelley, K.A. (2011) The oxidation state of Fe in MORB glasses and the oxygen fugacity of the upper mantle. Earth and Planetary Science Letters, 305, 270-282.

Cottrell, E., Kelley, K.A., Lanzirotti, A., and Fischer, R.A. (2009) High-precision determination of iron oxidation state in silicate glasses using XANES. Chemical Geology, 268, 167-179.

Cottrell, E., Birner, S.K., Brounce, M., Davis, F.A., Waters, L.E., and Kelley, K.A. (2020) Oxygen fugacity across tectonic settings. In D.R. Neuville, and R. Moretti, Eds. Redox variables and mechanisims in magmatism and volcanism, In Press. Wiley.

Dann, J.C., Holzheid, A.H., Grove, T.L., and McSween Jr., H.Y. (2001) Phase equilibria of the Shergotty meteorite: Constraints on pre-eruptive water contents of martian magmas and fractional crystallization under hydrous conditions. Meteoritics & Planetary Science, 36, 793-806.

Dreibus, G., Spettel, B., Haubold, R., Jochum, K.P., Palme, H., Wolf, D., and Zipfel, J. (2000) Chemistry of a new shergottite; Sayh al Uhaymir 005. Meteoritics & Planetary Science, 35, 49.

Dyar, M.D., Agresti, D.G., Schaefer, M.W., Grant, C.A., and Sklute, E.C. (2006) Mössbauer spectroscopy of Earth and planetary materials. Annual Review of Earth and Planetary Sciences, 34, 83-125.

Eastman, C.M., and Zhao, J.-C. (2019) Phase equilibria and diffusion in the Ni-Cr-Pt system at 1200 °C. Journal of Phase Equilibria and Diffusion, 40, 542-552.

Falloon, T.J., Danyushevsky, L.V., Ariskin, A., Green, D.H., and Ford, C.E. (2007) The application of olivine geothermometry to infer crystallization temperatures of parental liquids: Implications for the temperature of MORB magmas. Chemical Geology, 241, 207-233.

Filiberto, J. (2008) Experimental constraints on the parental liquid of the Chassigny meteorite: A possible link between the Chassigny meteorite and a Martian Gusev basalt. Geochimica et Cosmochimica Acta, 72, 690-701.

Filiberto, J., and Treiman, A.H. (2009) The effect of chlorine on the liquidus of basalt: First results and implications for basalt genesis on Mars and Earth. Chemical Geology, 263, 60-68.

Filiberto, J., and Dasgupta, R. (2011) Fe^{2+}-Mg partitioning between olivine and basaltic melts: Applications to genesis of olivine-phyric shergottites and conditions of melting in the Martian interior. Earth and Planetary Science Letters, 304, 527-537.

Filiberto, J., Treiman, A.H., and Le, L. (2008) Crystallization experiments on a Gusev Adirondack basalt composition. Meteoritics & Planetary Science, 43, 1137-1146.

Filiberto, J., Jackson, C., Le, L., and Treiman, A.H. (2009) Partitioning of Ni between olivine and an iron-rich basalt: Experiments, partition models, and planetary implications. American Mineralogist, 94, 256-261.

Filiberto, J., Dasgupta, R., Kiefer, W.S., and Treiman, A.H. (2010a) High pressure, near-liquidus phase equilibria of the Home Plate basalt Fastball and melting in the Martian mantle. Geophysical Research Letters, 37.

Filiberto, J., Musselwhite, D.S., Gross, J., Burgess, K., Loan, L.E., and Treiman, A.H. (2010b) Experimental petrology, crystallization history, and parental magma characteristics of olivine-phyric shergottite NWA 1068: Implications for the petrogenesis of ‘‘enriched’’ olivine-phyric shergottites. Meteoritics & Planetary Science, 45, 1258-1270.

Filiberto, J., Chin, E., Day, J.M.D., Franchi, I.A., Greenwood, R.C., Gross, J., Penniston-Dorland, S.C., Schwenzer, S.P., and Treiman, A.H. (2012) Geochemistry of intermediate olivine-phyric shergottite Northwest Africa 6234, with similarities to basaltic shergottite Northwest Africa 480 and olivine-phyric shergottite Northwest Africa 2990. Meteoritics & Planetary Science, 47, 1256-1273.

Filiberto, J., Gross, J., Udry, A., Trela, J., Wittmann, A., Cannon, K.M., Penniston-Dorland, S., Ash, R., Hamilton, V.E., Meado, A.L., Carpenter, P., Jolliff, B., and Ferré, E.C. (2018) Shergottite Northwest Africa 6963: A pyroxene-cumulate Martian gabbro. Journal of Geophysical Research: Planets, 123, 1823-1841.

Ford, C.E., Russell, D.G., Craven, J.A., and Fisk, M.R. (1983) Olivine-Liquid Equilibria: Temperature, Pressure and Composition Dependence of the Crystal/Liquid Cation Partition-Coefficients for Mg, Fe^{2+}, Ca and Mn. Journal of Petrology, 24, 256-265.

Fudali, R.F. (1965) Oxygen fugacities of basaltic and andesitic magmas. Geochimica et Cosmochimica Acta, 29, 1063-1075.

Funk, R.C. (2016) Petrology and geochemistry of new paired Martian meteorites LAR 12240 and LAR 12095. Department of Earth and Atmospheric Sciences, p. 118. University of Houston, Houston.

Gee, L.L., and Sack, R.O. (1988) Experimental petrology of melilite nephelinites. Journal of Petrology, 29, 1233-1255.

Goodrich, C.A. (2002) Petrogenesis of olivine-phyric shergottites Sayh al Uhaymir 005 and Elephant Moraine A79001 lithology A. In J. Jones, and D.W. Mittlehehldt, Eds. Unmixing the SNCs: Chemical, isotopic, and petrologic components of Martian meteorites, p. 17-18.

Goodrich, C.A., and Zipfel, J. (2001) Magmatic inclusions in olivine and chromite in basaltic shergottite Sayh al Uhaymir 005; implications for petrogenesis and relationship to lherzolitic shergottites. 32nd Lunar and Planetary Science Conference, abstract 1174.

Gross, J., Treiman, A.H., Filiberto, J., and Robinson, K. (2010) Primitive olivine-phyric shergottite NWA 5789: Petrography, mineral chemistry and cooling history imply a magma similar to Yamato 980459. 41st Lunar and Planetary Science Conference, abstract 1813.

Gross, J., Treiman, A.H., Filiberto, J., and Herd, C.D.K. (2011) Primitive olivine-phyric shergottite NWA 5789: Petrography, mineral chemistry, and cooling history imply a magma similar to Yamato-980459. Meteoritics & Planetary Science, 46, 116-133.

Gross, J., Filiberto, J., Herd, C.D.K., Daswani, M.M., Schwenzer, S.P., and Treiman, A.H. (2013) Petrography, mineral chemistry, and crystallization history of olivine-phyric shergottite NWA 6234: A new melt composition. Meteoritics & Planetary Science, 48, 854-871.

Grove, T.L. (1981) Use of FePt alloys to eliminate the iron loss problem in 1 atmosphere gas mixing experiments: Theoretical and practical considerations. Contributions to Mineralogy and Petrology, 78, 298-304.

Herd, C.D.K. (2003) The oxygen fugacity of olivine-phyric martian basalts and the components within the mantle and crust of Mars. Meteoritics & Planetary Science, 38, 1793-1805.

Herd, C.D.K., Dwarzski, R.E., and Shearer, C.K. (2009) The behavior of Co and Ni in olivine in planetary basalts: An experimental investigation. American Mineralogist, 94, 244-255.

Herd, C.D.K., Duke, M.J.M., Bryden, C.D., and Pearson, D.G. (2013) Tissint among the shergottites: Parental melt composition, redox state, La/Yb and V/Sc. 44th Lunar and Planetary Science Conference, abstract 2683.

Hsu, W., Wu, Y., and Jiang, Y. (2012) Petrology and mineralogy of the Tissint olivine-phyric shergottite. 75th Annual Meteoritical Society Meeting, abstract 5080.

Irving, A.J., Kuehner, S.M., Korotev, R.L., and Hupe, G.M. (2007) Petrology and bulk composition of primitive enriched olivine basaltic shergottite Northwest Africa 4468. 38th Lunar and Planetary Science Conference, abstract 1526.

Irving, A.J., Kuehner, S.M., Herd, C.D.K., Gellissen, M., Korotev, R.L., Puchtel, I., Walker, R.J., Lapen, T.J., and Rumble, D., III. (2010) Petrologic, elemental and multi-isotopic characterization of permafic olivine-phyric shergottite Northwest Africa 5789: A primitive magma derived from depleted Martian mantle. 41st Lunar and Planetary Science Conference, abstract 1547.

Irving, A.J., Kuehner, S.M., Ziegler, K., Chen, G., Herd, C.D.K., Conrey, R.M., Andreasen, R., Lapen, T.J., Hmani, M., and Hmani, A. (2013) Northwest Africa 7635: The first depleted, highly ferroan and phosphate-free evolved olivine-plagioclase-phyric shergottite. 76th Annual Meteoritical Society Meeting, abstract 5274.

Jayasuriya, K.D., O'Neill, H.S.C., Berry, A.J., and Campbell, S.J. (2004) A Mössbauer study of the oxidation state of Fe in silicate melts. American Mineralogist, 89, 1597-1609.

Jochum, K.P., Stoll, B., Herwig, K., Willbold, M., Amini, M., Arburg, S., Abouchami, W., Hellerbrand, E., Mocek, B., Raczek, I., Stracke, A., and Alard, O. (2006) MPI-DING reference glasses for in situ microanalysis: New reference values for element concentrations and isotopic ratios. Geochemistry, Geophysics, Geosystems, 7, Q02008, doi:1029/2005GC001060.

Kress, V.C., and Carmichael, I.S.E. (1988) Stoichiometry of the iron oxidation reaction in silicate melts. American Mineralogist, 73, 1267-1274.

Kress, V.C., and Carmichael, I.S.E. (1991) The compressibility of silicate liquids containing Fe_2O_3 and the effect of composition, temperature, oxygen fugacity and pressure on their redox states. Contributions to Mineralogy and Petrology, 108, 82-92.

Kuehner, S.M., Irving, A.J., Herd, C.D.K., Gellissen, M., Lapen, T.J., and Rumble, D., III. (2011) Pristine olivine-phyric shergottite Northwest Africa 6162: a primitive magma with accumulated crystals derived from depleted Martian mantle. 42nd Lunar and Planetary Science Conference, abstract 1610.

Lapen, T.J., Righter, M., Andreasen, R., Irving, A.J., Satkoski, A.M., Beard, B.L., Nishiizumi, K., Jull, A.J.T., and Caffee, M.W. (2017) Two billion years of magmatism recorded from a single Mars meteorite ejection site. Science Advances, 3, e1600922.

Longhi, J., Walker, D., and Hays, J.F. (1978) The distribution of Fe and Mg between olivine and lunar basaltic liquids. Geochimica et Cosmochimica Acta, 42, 1545-1558.

Matzen, A.K., Baker, M.B., Beckett, J.R., and Stolper, E.M. (2011) Fe–Mg partitioning between olivine and high-magnesian melts and the nature of Hawaiian parental liquids. Journal of Petrology, 52, 1243-1263.

McCanta, M.C., Elkins-Tanton, L., and Rutherford, M.J. (2009) Expanding the application of the Eu-oxybarometer to the lherzolitic shergottites and nakhlites: Implications for the oxidation state heterogeneity of the Martian interior. Meteoritics & Planetary Science, 44, 725-745.

McCubbin, F.M., Nekvasil, H., Harrington, A.D., Elardo, S.M., and Lindsley, D.H. (2008) Compositional diversity and stratification of the Martian crust: Inferences from crystallization experiments on the picrobasalt Humphrey from Gusev Crater, Mars. Journal of Geophysical Research-Planets, 113, E11013.

Médard, E., McCammon, C.A., Barr, J.A., and Grove, T.L. (2008) Oxygen fugacity, temperature reproducibility, and H_2O contents of nominally anhydrous piston-cylinder experiments using graphite capsules. American Mineralogist, 93, 1838-1844.

Mellin, M.J., Liu, Y., Schnare, D.W., and Taylor, L.A. (2008) Revised compositional estimate of EETA79001 lithology A groundmass. 39th Lunar and Planetary Science Conference, abstract 2150.

Mikouchi, T., Miyamoto, M., and McKay, G.A. (2001) Mineralogy and petrology of the Dar al Gani 476 martian meteorite: Implications for its cooling history and relationship to other shergottites. Meteoritics & Planetary Science, 36, 531-548.

Mikouchi, T., Kurihara, T., and Miyamoto, M. (2008) Petrology and mineralogy of RBT 04262: Implications for stratigraphy of the lherzolitic shergottite igneous block. 39th Lunar and Planetary Science Conference, abstract 2403.

Monders, A.G., Médard, E., and Grove, T.L. (2007) Phase equilibrium investigations of the Adirondack class basalts from the Gusev plains, Gusev crater, Mars. Meteoritics and Planetary Science, 42, 131-148.

Musselwhite, D.S., Dalton, H.A., Kiefer, W.S., and Treiman, A.H. (2006) Experimental petrology of the basaltic shergottite Yamato-980459: Implications for the thermal structure of the Martian mantle. Meteoritics & Planetary Science, 41, 1271-1290.

Mysen, B.O. (2006) Redox equilibria of iron and silicate melt structure: Implications for olivine/melt element partitioning. Geochimica et Cosmochimica Acta, 70, 3121-3138.

Nekvasil, H., McCubbin, F.M., Harrington, A., Elardo, S., and Lindsley, D.H. (2009) Linking the Chassigny meteorite and the Martian surface rock Backstay: Insights into igneous crustal differentiation processes on Mars. Meteoritics & Planetary Science, 44, 853-869.

O'Neill, H.S.C. (1987) Quartz-fayalite-iron and quartz-fayalite-magnetite equilibria and the free energy of formation of fayalite (Fe_2SiO_4) and magnetite (Fe_3O_4). American Mineralogist, 72, 67-75.

O'Neill, H.S.C., Berry, A.J., McCammon, C., Jayasuriya, K.D., Campbell, S.J., and Foran, G.J. (2006) An experimental determination of the effect of pressure on the $Fe^{+3}/\sum Fe$ ratio of anhydrous silicate melt to 3.0 GPa. American Mineralogist, 91, 404-412.

O'Neill, H.S.C., Berry, A.J., and Mallmann, G. (2018) The oxidation state of iron in Mid-Ocean Ridge Basaltic (MORB) glasses: Implications for their petrogenesis and oxygen fugacities. Earth and Planetary Science Letters, 504, 152-162.

Papike, J.J., Karner, J.M., Shearer, C.K., and Burger, P.V. (2009) Silicate mineralogy of martian meteorites. Geochimica et Cosmochimica Acta, 73, 7443-7485.

Peslier, A.H., Hnatyshin, D., Herd, C.D.K., Walton, E.L., Brandon, A.D., Lapen, T.J., and Shafer, J.T. (2010) Crystallization, melt inclusion, and redox history of a Martian meteorite: Olivine-phyric shergottite Larkman Nunatak 06319. Geochimica et Cosmochimica Acta, 74, 4543-4576.

Pouchou, J.-L., and Pichoir, F. (1988) A simplified version of the "PAP" model for matrix corrections in EPMA. In D.E. Newbury, Ed. Microbeam Analysis, p. 315-318. San Francisco Press, San Francisco.

Putirka, K.D., Perfit, M., Ryerson, F.J., and Jackson, M.G. (2007) Ambient and excess mantle temperatures, olivine thermometry, and active vs. passive upwelling. Chemical Geology, 241, 177-206.

Righter, K., Danielson, L.R., Pando, K., Morris, R.V., Graff, T.G., Agresti, D.G., Martin, A.M., Sutton, S.R., Newville, M., and Lanzirotti, A. (2013) Redox systematics of martian magmas with implications for magnetite stability. American Mineralogist, 98, 616-628.

Roeder, P.L., and Emslie, R.F. (1970) Olivine-liquid equilibrium. Contributions to Mineralogy and Petrology, 29, 275-289.

Sack, R.O., Carmichael, I.S.E., Rivers, M., and Ghiorso, M.S. (1980) Ferric-ferrous equilibria in natural silicate liquids at 1bar. Contributions to Mineralogy and Petrology, 75, 369-376.

Sarbadhikari, A.B., Day, J.M.D., Liu, Y., Rumble, D., and Taylor, L.A. (2009) Petrogenesis of olivine-phyric shergottite Larkman Nunatak 06319: Implications for enriched components in martian basalts. Geochimica et Cosmochimica Acta, 73, 2190-2214.

Seifert, S., O'Neill, H.S.C., and Brey, G. (1988) The partitioning of Fe, Ni and Co between olivine, metal, and basaltic liquid: An experimental and thermodynamic investigation, with application to the composition of the lunar core. Geochimica et Cosmochimica Acta, 52, 603-616.

Shearer, C.K., McKay, G.A., Papike, J.J., and Karner, J.M. (2006) Valence state partitioning of vanadium between olivine-melt: Estimates of the oxygen fugacity of Y980459 and application to other olivine-phyric martian basalts. American Mineralogist, 91, 1657-1663.

Shirai, N., and Ebihara, M. (2004) Chemical characteristics of a Martian meteorite, Yamato 980459. Antarctic Meteorite Research, 17, 55-67.

Shirai, N., Humayun, M., and Irving, A.J. (2009) The bulk composition of coarse-grained meteorites from laser ablation analysis of their fusion crusts. 40th Lunar and Planetary Science Conference, abstract 2170.

Sossi, P.A., Klemme, S., O'Neill, H.S.C., Berndt, J., and Moynier, F. (2019) Evaporation of moderately volatile elements from silicate melts: experiments and theory. Geochimica et Cosmochimica Acta, 260, 204-231.

Stolper, E. (1977) Experimental petrology of eucritic meteorites. Geochimica et Cosmochimica Acta, 41, 587-611.

Taylor, L.A., Nazarov, M.A., Shearer, C.K., McSween, H.Y., Cahill, J., Neal, C.R., Ivanova, M.A., Barsukova, L.D., Lentz, R.C., Clayton, R.N., and Mayeda, T.K. (2002) Martian meteorite Dhofar 019: A new shergottite. Meteoritics & Planetary Science, 37, 1107-1128.

Thornber, C.R., Roeder, P.L., and Foster, J.R. (1980) The effect of composition on the ferric-ferrous ratio in basaltic liquids at atmospheric pressure. Geochimica et Cosmochimica Acta, 44, 525-532.

Toplis, M.J. (2005) The thermodynamics of iron and magnesium partitioning between olivine and liquid: criteria for assessing and predicting equilibrium in natural and experimental systems. Contributions to Mineralogy and Petrology, 149, 22-39.

Tsuchiyama, A., Nagahara, H., and Kushiro, I. (1981) Volatilization of sodium from silicate melt spheres and its application to the formation of chondrules. Geochimica et Cosmochimica Acta, 45, 1357-1367.

Tuff, J., Wade, J., and Wood, B.J. (2013) Volcanism on Mars controlled by early oxidation of the upper mantle. Nature, 498, 342-345.

Usui, T., McSween, H.Y., and Floss, C. (2008) Petrogenesis of olivine-phyric shergottite Yamato 980459, revisited. Geochimica et Cosmochimica Acta, 72, 1711-1730.

Virgo, D., and Mysen, B.O. (1985) The structural state of iron in oxidized vs. reduced glasses at 1 atm: A ^{57}Fe Mössbauer study. Physics and Chemistry of Minerals, 12, 65-76.

Zhang, H.L., Cottrell, E., Solheid, P.A., Kelley, K.A., and Hirschmann, M.M. (2018) Determination of $Fe^{3+}/\Sigma Fe$ of XANES basaltic glass standards by Mössbauer spectroscopy and its application to the oxidation state of iron in MORB. Chemical Geology, 479, 166-175.

Zipfel, J., Scherer, P., Spettel, B., Dreibus, G., and Schultz, L. (2000) Petrology and chemistry of the new shergottite Dar al Gani 476. Meteoritics & Planetary Science, 35, 95-106.

This is the peer-reviewed, final accepted version for American Mineralogist, published by the Mineralogical Society of America.
The published version is subject to change. Cite as Authors (Year) Title. American Mineralogist, in press.
DOI: https://doi.org/10.2138/am-2021-7682. http://www.minsocam.org/

Table 1. Starting Compositions in wt. %

Sample	n[a]	SiO_2	TiO_2	Al_2O_3	Cr_2O_3	FeO*[b]	MnO	MgO	CaO	Na_2O	K_2O	NiO	Sum
Prim. Home Plate Avg.[c]		49.42	0.98	9.84	-	17.78	0.35	11.57	6.51	3.12	0.43	–	100
MB1[d]		51.01	1.01	10.15	0.0	18.36	0.36	11.94	6.72	0.0	0.0	0.45	100
Syn-MB1[e]		51.01	1.00	10.15	0.0	18.36	0.36	11.94	6.72	0.0	0.0	0.46	100
Syn-MB1 Exp. Avg[f]	107	50.33(28)	1.00(3)	10.09(8)	BDL	18.13(31)	0.37(4)	11.76(9)	6.89(8)	0.06(2)[g]	BDL	0.33(8)[h]	98.96
Syn-MB2[i]		48.36	0.83	8.36	0.0	18.86	0.301	16.62	5.71	0.0	0.0	0.38	100
Syn-MB2 gl[j]	20	50.13(11)	0.94(3)	9.46(8)	BDL	18.61(18)	0.32(4)	13.03(8)	6.54(8)	0.10(1)	BDL	0.21(3)	99.35
Syn-MB2 ol	15	38.92(14)	BDL	BDL	BDL	18.50(10)	0.25(1)	41.17(16)	0.16(1)	BDL	–	1.53(5)	100.55

[a] Number of analyses used to generate the average.

[b] All Fe as FeO.

[c] Average of Home Plate primitive magma compositions reported in Filiberto and Dasgupta (2011).

[d] Target composition after replacement of K_2O with an equal amount of NiO and renormalization on an alkali-free basis.

[e] As-weighed composition.

[f] Average of 107 analyses from 12 experiments. Numbers in parenthesis are analytical uncertainties in terms of the least units cited, e.g., entry 50.33(28) for sample "Syn-MB1 Exp. Avg" corresponds to 50.33 ± 0.28 where 0.28 is the standard deviation of the 107 measurements.

[g] The average and standard deviation for Na_2O includes only those experiments where Na_2O was above the detection limit: experiments 11, 13, 57, 60, and 61

[h] The average and standard deviation for NiO excludes the two experiments 30 and 57 where NiO was below the detection limit.

[i] Mixture of 83% syn-MB1 experimental average with 17% synthetic Fo_{77} olivine. Due to possible Fe, and Ni loss, as well as Na gain, the concentration of these elements were calculated using the theoretical syn-MB1 values.

[j] Composition of coexisting glass and olivine from experiment 2-3 using syn-MB2 starting material run at 1300°C and a $\log_{10}fO_2$ of -7.24 for 41.25 hrs.

Abbreviations: BDL = below detection limit; dash indicates that the element in question was not analyzed or reported.

This is the peer-reviewed, final accepted version for American Mineralogist, published by the Mineralogical Society of America.
The published version is subject to change. Cite as Authors (Year) Title. American Mineralogist, in press.
DOI: https://doi.org/10.2138/am-2021-7682. http://www.minsocam.org/

Table 2. Run conditions and experimental results

Run#	Temp (°C)	Time (hrs)	logfO_2[a]	Loop # & usage[b]	ΔFeO* % [c]	ΔNiO wt. %[d]	ΔNa_2O wt. %[e]	$Fe^{3+}/\sum Fe$ Mthd A[f]	$Fe^{3+}/\sum Fe$ Mthd B[f]
7	1458	15.5	–0.68	Pt1/3	–1.00	–0.01	-	0.69	0.66
11	1451	48.6	–5.88	Pt3/3	–0.95	–0.20	0.07	0.19	0.08
13	1450	23.3	–5.85	Pt3/4	–0.82	–0.14	0.05	0.19	0.09
15	1451	13.5	–5.87	Pt3/5	0.20	–0.09	-	0.19	0.09
20	1451	12.5	–4.76	Pt4/3	–1.17	–0.05	-	0.25	0.16
21	1451	13.4	–2.48	Pt5/3	0.14	–0.05	-	0.44	0.38
27	1450	8.5	–8.0	Re1/2	0.12	–0.17	-	0.06	0.01
30	1449	14.4	–10.0	Re2/2	–5.70	–0.46	-	0.06	0.00
31	1500	10.5	–4.9	Pt6/2	–1.10	–0.07	-	0.22	0.13
57	1451	11.0	–10.03	Re16/2	–3.00	–0.46	0.08	0.07	0.00
60	1452	9.5	–8.20	Re18/2	–0.73	–0.25	0.05	0.06	0.01
61	1300	36.1	–7.20	Pt14/3	–1.40	–0.14	0.06	0.19	0.09
2-3	1300	41.2	–7.24	Pt14/5	–2.06	–0.02	0.09		

[a] Oxygen fugacity measurements are reported to two decimal places; oxygen fugacities from gas mixing ratios are reported to only one, excepting the experiment performed in air.
[b] Loop material and loop designation number followed by the number of experiments that had been run with the loop prior to the present experiment.
[c] Relative change (in percent) of FeO* in the bulk composition, where FeO* indicates the wt.% of all Fe in the glass computed as FeO, based on mass balance; negative sign denotes a decrease in FeO*.
[d] Change in NiO (in wt. %) to the bulk composition based on the NiO content of the glass and mass balance. NiO in runs 30 and 57 was below the detection limit (~0.08 wt. % NiO); hence, a reported value equal to the bulk NiO, 0.46 wt. %.
[e] Change in Na_2O (in wt. %) based on the Na_2O content of the glass; a dash indicates that Na was below the detection limit.
[f] Estimated error on $Fe^{3+}/\sum Fe$ is 0.03, a value that contains both error in the fit and any systematic error.

Note: Mass-balance calculations used the non-linear approach of Albarède & Provost (1977), see Matzen et al. (2011) for more details. Mass-balance calculations for Run 2-3 yield 88% liquid and 12% olivine (by weight).

This is the peer-reviewed, final accepted version for American Mineralogist, published by the Mineralogical Society of America.
The published version is subject to change. Cite as Authors (Year) Title. American Mineralogist, in press.
DOI: https://doi.org/10.2138/am-2021-7682. http://www.minsocam.org/

Table 3. Hyperfine Parameters

	Doublet 1 Fe^{2+}			Doublet 2 Fe^{2+}			Doublet 3 Fe^{3+}				
Run #	IS	QS	σcs	IS	QS	σcs	IS	QS	σcs	$Fe^{3+}/\sum Fe$	χ^2
Method A											
7	1.14	2.28	0.16	1.02	1.72	0.25	0.29	1.33	0.27	0.69	1.70
11	1.18	2.32	0.17	1.05	1.84	0.26	0.46	1.38	0.32	0.19	1.43
13	1.17	2.31	0.18	1.05	1.82	0.26	0.47	1.37	0.30	0.19	1.49
15	1.16	2.33	0.17	1.05	1.8	0.25	0.44	1.4	0.30	0.19	1.22
20	1.18	2.32	0.17	1.05	1.83	0.26	0.38	1.34	0.30	0.25	1.34
21	1.17	2.33	0.16	1.05	1.79	0.26	0.32	1.32	0.27	0.44	1.48
27	1.14	2.16	0.22	1.01	1.78	0.30	0.58	1.11	0.14	0.06	1.29
30	1.15	2.19	0.21	1.02	1.79	0.29	0.62	1.19	0.14	0.06	1.21
31	1.17	2.32	0.17	1.05	1.83	0.26	0.41	1.36	0.29	0.22	1.22
57	1.16	2.23	0.20	1.03	1.82	0.28	0.63	1.18	0.15	0.07	1.13
60	1.15	2.16	0.21	1.01	1.81	0.30	0.59	1.08	0.14	0.06	1.18
61	1.16	2.32	0.17	1.05	1.83	0.26	0.48	1.38	0.31	0.19	1.48
Method B											
7							0.29	1.32	0.27	0.66	1.86
11							0.27	1.33	0.21	0.08	1.41
13							0.31	1.33	0.22	0.09	1.46
15							0.29	1.33	0.24	0.09	1.36
20							0.28	1.31	0.24	0.16	1.42
21							0.29	1.30	0.26	0.38	1.60
27							0.44	1.08	0.02	0.01	1.27
30										0.00	
31							0.28	1.32	0.23	0.13	1.18
57							0.30	1.33	0.06	0.00	1.18
60							0.14	1.63	0.00	0.01	1.11
61							0.29	1.34	0.24	0.08	1.39

Note: Isomer shift (IS), quadrupole splitting (QS) and Gaussian distribution width (σcs) are in mm/s. All spectra acquired at room temperature, and fit with Lorentzian widths set =0.19 mm/s. Method A used two Fe^{2+} and one Fe^{3+} doublet; Method B—meant to simulate the approach of Berry et al. (2018) —used three Fe^{2+} doublets, and one Fe^{3+} doublet. The three Fe^{2+} doublets used in Method B used hyperfine parameters obtained by fitting the most reduced experiment (Run # 30). IS, QS, and σcs of the three doublets fit to Run #30 are 1.15, 2.19, 0.21; 1.02, 1.79, 0.29; 0.62, 1.19, 0.14, respectively.